12-2018

Plasmonic Enhancement of Photoluminescence and Photobrightening in CdSe Quantum Dots

David Alan French
University of Arkansas, Fayetteville

Plasmonic Enhancement of Photoluminescence and Photobrightening in CdSe Quantum Dots

A dissertation submitted in partial fulfillment
of the requirements for the degree of
Doctor of Philosophy in Physics

by

David French
Rose-Hulman Institute of Technology
Bachelor of Science in Physics, 2011
University of Arkansas
Master of Science in Physics, 2015

December 2018
University of Arkansas

This dissertation is approved for recommendation to the Graduate Council.

_____
Joseph B. Herzog, Ph.D.
Dissertation Director

_____
Hugh Churchill, Ph.D.
Committee Member

_____
William Harter, Ph.D.
Committee Member

Abstract

Quantum dots are gaining recognition not just in the physics and chemistry community, but in the public eye as well. Quantum dot technologies are now being used in sensors, detectors, and even television displays. By exciting quantum dots with light or electricity, they can be made to emit light, and by altering the quantum dot characteristics the wavelength can be finely tuned. The light emitted can be also be made more intense by an increase in the excitation energy. The excitation light can be increased via plasmonic enhancement, leading to increased luminescence. Aside from the relatively steady-state response, quantum dots also have several time-dependent behaviors – blueing, blinking, brightening, and bleaching. Brightening has several factors which affect it and is the focus of this work. This dissertation explores one of the factors which contributes to the photobrightening, namely the intensity of the excitation light, and examines the possibility of enhancing the emitted light via a range of plasmonic geometries. Gold nanoparticles come in many shapes and sizes and are ideally suited for enhancing light in the visible wavelength. By combining gold nanoparticles with cadmium selenide quantum dots, it is possible to enhance the photobrightening effect, potentially leading to better, more effective quantum dot technologies.

Acknowledgements

I'd like to thank my dissertation director, Dr. Joseph Herzog, for your support and guidance through the many years of my graduate school research, both personal and professional for pushing me at times when I would not push myself. It has been an honor to be part of your first group of graduate students, to start a lab from scratch and grow with it over the years. I'd also like to thank the other members of my committee, Dr. William Harter and Dr. Hugh Churchill, for their advice as I worked to find a direction of interest for my research.

Thanks to my group members, past and present, who provided assistance over the years, especially Stephen Bauman, Ahmad Darweesh, and Desalegn Debu, who have worked with me over the past many years, giving assistance with everything from electron microscopes to COMSOL models. Thanks to Gabrielle Abraham, Chandler Bernard, and Madison Whitby, whose work in the lab provided much of the initial background necessary for the research.

Special thanks are owed to Dr. Colin Heyes for providing the quantum dots used here free of charge, and also to Dr. Mark Knight for his insights into the issues with our optical setup. The assistance provided by these two has been invaluable and, quite literally, priceless.

My thanks to my fellow physics graduate students for providing camaraderie and moral support over the years, as well as assistance with studying concepts with which I was unfamiliar. Without them, I would not have been able to survive the classes. My thanks also to my fellow teaching assistants and my undergraduate students, for providing me a much-looked-forward-to break from my research to go and enjoy a few hours of learning by teaching. Along with this go my thanks for the Physics Department itself for providing me a teaching assistantship every year. The money received pales in comparison to the joy provided. Thanks to Dr. Gay Stewart for seeing in me the teacher that she knew I could become.

Finally, thanks to my parents and brother for everything you have given me my whole life. You have given me an inquisitive spirit and the desire never to quit. I wouldn't be who I am as a person without you. I hope I've made you proud.

Last, and certainly most, thanks to my wonderful wife Christine. You are the best thing that has ever happened to me. Sorry I took so long. Thanks for everything.

Table of Contents

Table of Figures

Table of Tables

CHAPTER I. INTRODUCTION

i. Plasmonics

When light is incident on a conductive surface, the electromagnetic field of the light can interact with the free electrons in the conductor, causing the electrons to begin to move opposite to the direction of the electric field[1], [2]. As light is an oscillating electric field, the direction in which the electrons are forced will oscillate as well, causing an out-of-phase oscillation in the electrons. If the frequency of the incoming EM field is the right frequency, depending on the material type and geometry of the target structure, the electrons can begin to oscillate as a group. This collection of oscillating electrons is called a plasmon[3]. As plasmons are a group of electric charges, they have their own electric field. The oscillation of the plasmon can therefore create its own oscillating electric field (light)[4], as shown in Figure 1.

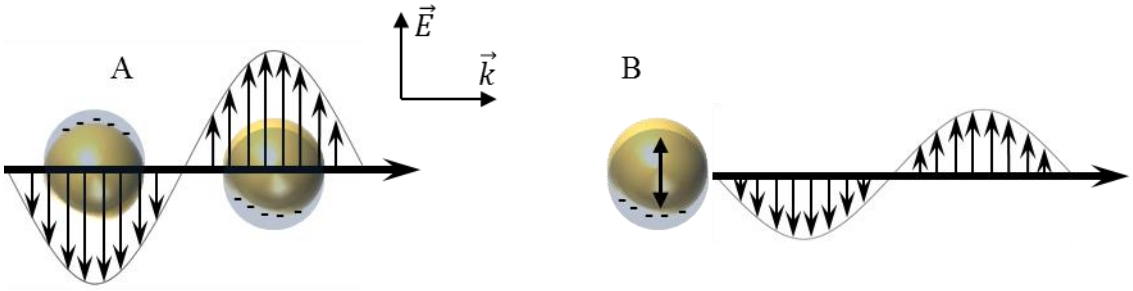

Figure 1 (A) A ray of light is incident on metallic nanospheres from the left, causing the electrons to be displaced by the field. (B) The electrons oscillate across (the vertical arrow) the nanosphere when returning to their original states, causing a ray of light to be emitted of the same wavelength as the incoming light. The lower magnitude is due to non-radiative losses in the sphere.

This light from the plasmon will be the same frequency, although obviously not wavelength, as that of the plasmon, which is, in turn, the same frequency of the incoming light. As the light is not changed in frequency, it can rightly be referred to as scattered light. The strength of this scattered light is dependent upon the maximum intensity of the plasmonic field, meaning

that more light will be scattered toward the point where the most electrons will gather, as per normal electric field distributions[5]. The result of this is that, despite the incident light intersecting a large portion of the conductive structure, the scattered light comes primarily from just a few spots, in effect, moving the light from all over the nanostructure to a very small area. The net outcome is a large optical enhancement of the light in a very small area, allowing for light to be focused below the diffraction limit[6] and creating a much greater maximum electromagnetic field than would otherwise be feasible. The benefits of this are numerous, including enhanced photovoltaics[7]–[9], sensors[10]–[14], photodetectors[15], and surface-enhanced Raman spectroscopy[16]–[18].

The primary goals when designing a device are to maximize the optical enhancement and tune the device for specific wavelengths of light. The wavelengths of light which respond best are the resonant wavelengths. The resonant wavelength of a plasmonic device can be altered via many characteristics, including size[19], shape[5], material, and surrounding medium[20]. Altering these characteristics allows tuning of the plasmonic resonant wavelength across a wide range of frequencies in order to suit the desired task.

The main concern of plasmonics, however, is the optical enhancement. Optical enhancement is the ratio of the intensity of the light after the plasmonic interaction to the intensity of the incoming light at a given location. As the intensity of light is proportional to the square of the magnitude of the electric field, the optical intensity can also be written as the square of the ratio of the plasmonically-enhanced electric field to the incoming field. Due to advances in computer simulations, it has become significantly easier in the last decade to create simulations of

nanoparticles of various sizes and compute their plasmonic response to light. The optical enhancement can be easily determined by solving Maxwell's equations over a defined mesh using either finite-element methods[5], [10], [15], [19], [21] or finite-difference methods[22], [23]. Nevertheless, these are but simulations of the structures, reliant upon the ability of the programmers to apply proper simulation methods and the user to construct simulation spaces that most closely resemble the structures which will be fabricated; structures which will, with little doubt, have variations diminishing the accuracy of the simulations. Possible though it is to use currently available methods such as near-field scanning optical microscopes to determine the spectrum of the plasmonically enhanced light, such methods are costly. An experimental method using material effects to test the optical characteristics, such as that presented here, would be significantly cheaper as well as give a result which would more closely resemble a real-world use case. In this work, quantum dots will be used for the characterizing material.

ii. Quantum Dots

Quantum dots are nanostructures just a few nanometers across which can function as three-dimensional quantum wells[24]. They are semiconductors which are able to emit light when an outside electric field is applied to them, either through electricity or an exciting light. In the case of exciting light, the incoming light is absorbed by the quantum dot, causing an electron to be excited into a higher energy state. The electron is then able to recombine with the hole that it previously left; this recombination results in a photon being emitted, as shown in Figure 2.

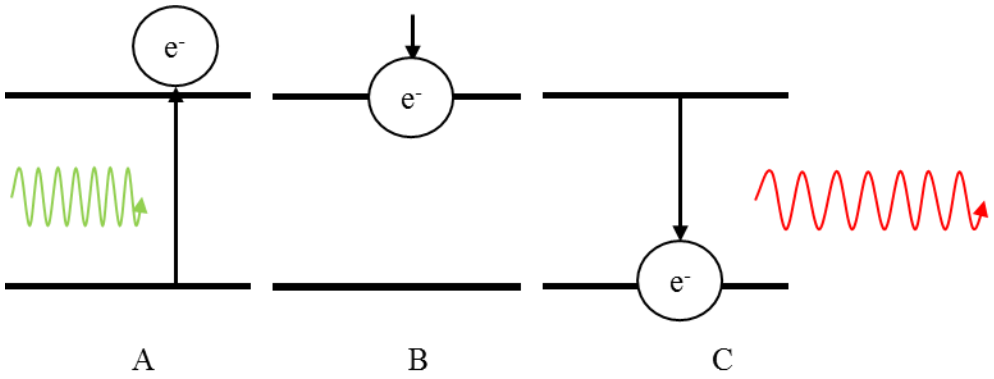

Figure 2 (A) A photon is absorbed by an atom, causing an electron to gain energy. This gain in energy pushes it to a higher energy state. (B) The photon settles to an allowed energy state, giving off some of its energy in non-radiative losses such as vibrational (thermal) energy. (C) The electron falls back to its original energy level, releasing a photon. This photon is of a lower energy than the original photon due to the losses in (B).

The energy absorbed by the electron is typically greater than the energy of the emitted photon; the difference is accounted for by non-radiative losses. The energy of the incoming light need only be greater than the band gap to excite the electron, meaning that the incoming light can be of any wavelength sufficiently short. The emitted light is determined exclusively by the size, shape, and composition of the quantum dot. This means that quantum dots are highly tunable[25], making them ideal for a wide variety of uses, including sensing[26], biomedical imaging[27], light-emitting diodes[28]–[30], and solar cells[31]–[33]. The intensity of the emitted light is affected by several factors, including temperature[34], [35], size[36], and intensity of the incoming light[37]. It is this last characteristic which makes plasmonics an intriguing combination. When combined with plasmonic nanostructures, the quantum dots have a vastly increased excitation energy, and thus a vastly increased emission signal. This behavior has been well examined in many studies[37]–[39]. It is worth a note that all of these behaviors are snap shot images. In other words, these are not repeated measurements on the same region. The reason for this is that quantum dots can have time-dependent behaviors such as blinking[40], [41], blueing[42]–[44],

bleaching[44], [45], and brightening[24], [37], [39], [46]–[49]. Of these, the focus here is on brightening. Photobrightening, or photoenhancement as it is sometimes known[47], [50], [51], is the process by which the intensity of the luminescence of a quantum dot increases over time due to continued exposure to excitation light. The mechanism behind this is not well understood, but [46], [47] suggest that a permanent chemical change takes place, causing a sealing effect (known as passivation) on charge-carrier traps. Other work indicates that it could be a thermal effect[52]; the addition of thermal energy leads to phonon contributions, causing an increased probability of a photon being emitted. The photobrightening should increase with increased excitation intensity, meaning that a plasmonic contribution should also cause an increase in the photobrightening. The two mechanisms named here which might cause photobrightening each would be enhanced by different plasmonic effects of nanoparticles. Optical passivation would be enhanced by the scattering spectrum of the nanoparticles while thermal effects would be enhanced by the absorption profile[53]. The combination of quantum dots and nanoparticles can therefore be used to determine the plasmonic effects by studying the change in the photobrightening of the quantum dots.

The combination of quantum dots and nanoparticles is not unique; it has been studied repeatedly[37], [39], [54]. Importantly, Chen's work[54] has studied the plasmonic effects on photobrightening. The conclusion reached there is that the presence of gold nanoparticles dampens out all photobrightening. The quantum dots in that paper photobrighten without nanoparticles; with the addition of nanoparticles the photobrightening is eliminated. This damping effect is attributed to quenching of the photoluminescence effect through energy transfer. While quenching between quantum dots and gold nanoparticles can happen[41], it is not a guarantee, and indeed

there are papers which have combined quantum dots with plasmonic nanoparticles and not had quenching cause such extensive trouble[37], [39], [49]. The paper by Chen, et al.[54] does not provide a sufficient amount of information to determine the reason why quenching was such an issue. It is worth noting, however, that Chen's paper provides a use for quenching, i.e. distinguishing between electron transfer, which does not cause quenching, and energy transfer, which does.

In light of all previous studies, the combination of nanoparticles and quantum dots begs three important questions. The first is the relation between photobrightening and laser intensity. While there have been previous studies of photobrightening which have shown that continuous light causes greater photobrightening than pulsed light[55], there remains still the unanswered question of how the photobrightening varies with the excitation intensity. Next is to determine if nanoparticles can enhance the photobrightening or if the photobrightening rate will, as shown by Chen, quench all photobrightening. Finally, if the nanoparticles do enhance photobrightening, by what mechanism do they enhance it, and, more importantly, can that enhancement factor be used to characterize future nanostructures.

CHAPTER II. METHODOLOGY

i. Sample Preparation

The quantum dots being used in these experiments are prepared using methods outlined in [41]. A diagram of the cross-section of a quantum dot is shown in Figure 3.

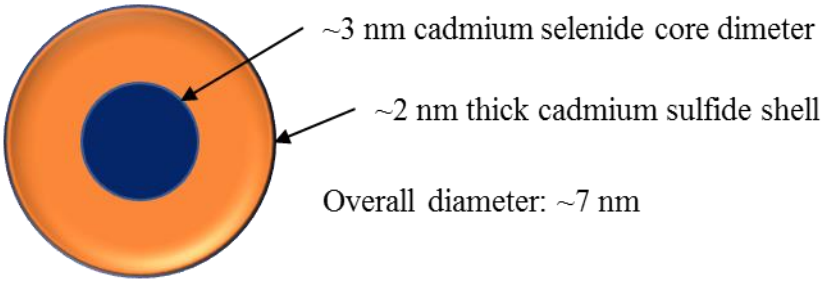

Figure 3 A cross-section of a quantum dot. The core is a 3 nm CdSe sphere while the outside shell is CdS. A protective layer of ligands surrounds the quantum dot, which is not shown on this diagram.

These quantum dots also have a protective layer of ligands surrounding each one in order to keep them from being quenched by the gold nanoparticles. The diameter of the core and shell gives a photoluminescence peak around 627 nm. An example of the emission spectrum is shown in Figure 4.

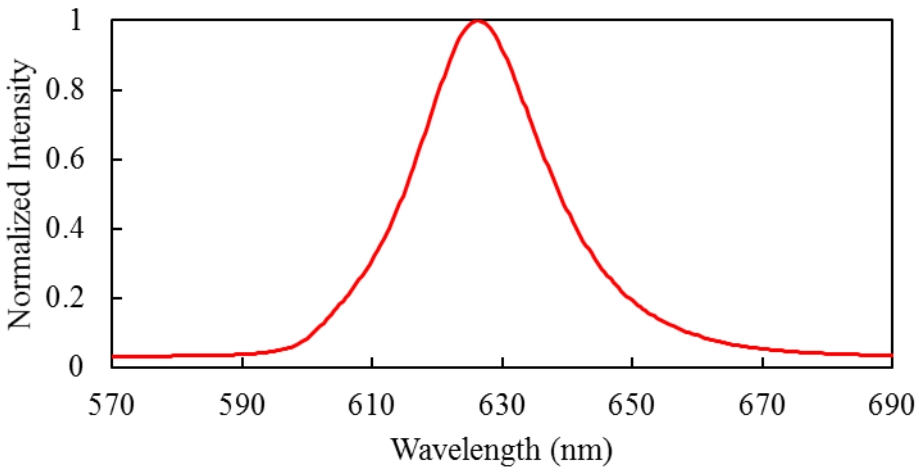

Figure 4 An example of the emission spectrum of a quantum dot determined via photoluminescence. The spectrum has been normalized to its maximum value.

There will be some variation in the quantum dots, even within a single batch. To keep the results between quantum dot samples as consistent as possible, a single batch of quantum dots was procured, and all samples were prepared from that batch.

For the nanoparticle studies, each sample is prepared in the same manner. The sample substrates are silicon chips with a native oxide layer of approximately 15 angstroms. The substrates are previously coated in a layer of poly(methyl methacrylate) (PMMA) to protect the chips against contamination. The PMMA is removed via a one-hour acetone soak prior to deposition. After the acetone soak, the chip is sonicated for one minute in acetone. Once sonicated, the chip is rinsed with acetone and then with isopropyl alcohol. It is then blown dry using compressed nitrogen.

The quantum dots are suspended in hexane at a molarity of 3.642×10^{-6} and stored at 4 °C in a dark environment in order to keep the quantum dots from being activated by either light or

heat, improving their lifetime and ensuring the initial intensity of the quantum dots remains as constant as possible, barring the effects of long-term decreases, which are unable to be eliminated. Prior to deposition, they are sonicated in a heated bath for one minute to create an even distribution. A dropper is used to deposit a single drop of quantum dot solution on the cleaned silicon substrate. In the case where a mixture of nanoparticles and quantum dots are desired, the nanoparticle solution is first sonicated for 30 seconds and then a single drop of nanoparticle solution is deposited on top of the quantum dot solution. The reason for the ordering of the deposition is to more closely reflect the methodology in both [37] and [54]. The sample is then left to dry for at least 48 hours. The reason for the drying period is two-fold. The first is that, though the quantum dots are suspended in hexane and thus dry quickly, the gold nanoparticles are suspended in deionized water, a much more slowly drying substance. The water must necessarily evaporate prior to mounting the sample so that the nanoparticles will be at the surface of the substrate so that they will interact with the quantum dots rather than be free-floating. The second reason is that, during the course of running experiments with samples which had not fully dried, it was discovered that the quantum dots have a tendency to photobleach rather than photobrighten. Over time the photobrightening behavior does reappear, indicating perhaps that the sample is quickly drying. This would tend to push the explanation of photobrightening toward the idea that the thermal effect is a dominant factor in the photobrightening, as the thermal contributions would necessarily be lowered while the water is present to absorb the excess thermal energy. The absorption of thermal energy would then encourage the quicker evaporation of the water, leading to photobrightening. The deposition process is illustrated in Figure 5. Once this is completed, the sample is ready for characterization.

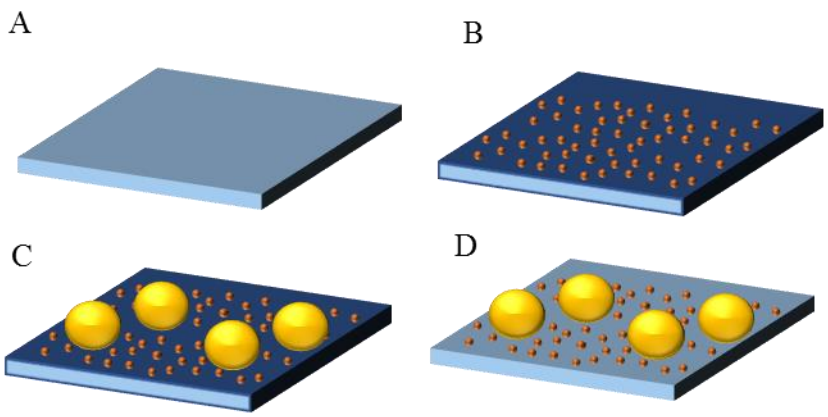

Figure 5 Sample preparation method. The substrate (A) is cleaned with acetone and isopropyl alcohol. Quantum dots are then deposited (B). After this, the desired nanoparticles are deposited (C) and the sample is then left to dry (D) for 48 hours.

ii. Photoluminescence

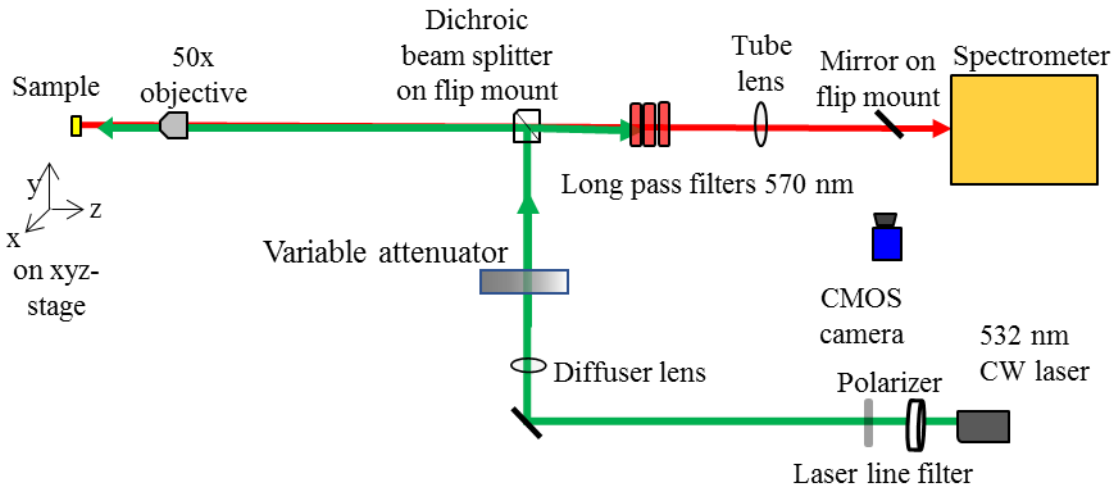

Figure 6 The photoluminescence experimental design. The green path is the excitation light and the red path is the emitted light. The light path to the camera is not pictured. Light emitted by the laser is passed though a line filter to remove secondary and tertiary laser lines, then polarized. It is focused onto the back of an objective though an attenuator and beam splitter. The light is then sent to the sample through the objective, resulting in a spot size of 50 microns. Upon hitting the sample, the excitation light and newly emitted light are directed back through the objective, through the dichroic beam splitter and a set of long pass filters. These remove most of the excitation light from the signal. The remaining light is focused onto either the spectrometer or CMOS camera via a tube lens.

Figure 6 shows the optical design for testing photoluminescence. The sample is attached to a motorized XYZ stage to enable repositioning as well as focusing. A 532 nm, 5 mW laser is directed through a laser line filter to restrict the laser to a single wavelength and a polarizer to ensure vertical polarization. A 200 mm focal length lens is placed in the path which focuses the laser on the back of the objective; this causes the beam to diverge in the objective, creating a larger than normal beam spot. The final beam spot has an area of roughly 1.07×10^5 cm^2. After the lens, the laser is attenuated by a variable optical density filter. This filter has optical density values which run from 0.0 to 4.0; the optical densities and resultant intensities are noted in Table 1. The power values reported are measured at the surface of the sample. Prior to taking measurements, the laser is turned on and allowed to stabilize its power over the course of an hour. This is necessary as the laser power stabilizes at a value of 2.5 W, or half of the initial power.

Table 1 Laser intensity for each optical density

Optical Density	Power (μW)	Intensity (W/cm2)
0.0	210	19.6
0.1	180	16.8
0.2	143	13.3
0.3	105	9.79
0.4	82.1	7.66
0.5	62.8	5.86
0.8	32.1	2.99
1.0	18.6	1.74
2.0	1.13	0.105
3.0	0.242	0.0226
4.0	0.159	0.0148

A dichroic beam splitter reflects the laser to the objective; upon return it helps to filter out some of the laser light. The laser is then passed through a 50x microscope objective whereby it is defocused onto the sample. Once the excitation light hits the sample, the majority of it is scattered

and reflected back into the microscope objective along with the emitted light from the quantum dots. The light is then collimated by the objective and directed toward the spectrometer. Passing through the dichroic beam splitter and three long-pass filters cuts out the vast majority of the excitation light, leaving only the emitted light. A 200 mm focal lens is then used to focus the light onto the slit of the spectrometer. There is also a mirror on a flip mount which can be put in place to redirect the light to a CMOS camera, placed at an equidistance from the camera and spectrometer slit, meaning that if the image is in focus in the camera it will also be in focus for the spectrometer. This is a true-color camera which is used for alignment and focusing of the samples. To focus the sample, the diffuser lens is removed, meaning that the laser will be roughly collimated going into the back of the microscope objective. The objective will therefore focus the laser at the focal point of the objective, meaning that when the laser is in focus on the camera the sample will be as well. The laser is in focus when a characteristic diffraction pattern is present in the view of the camera. Once focused, the diffuser lens is replaced and the flip mount mirror is lowered so as not to block the beam path to the spectrometer.

iii. Spectrometer

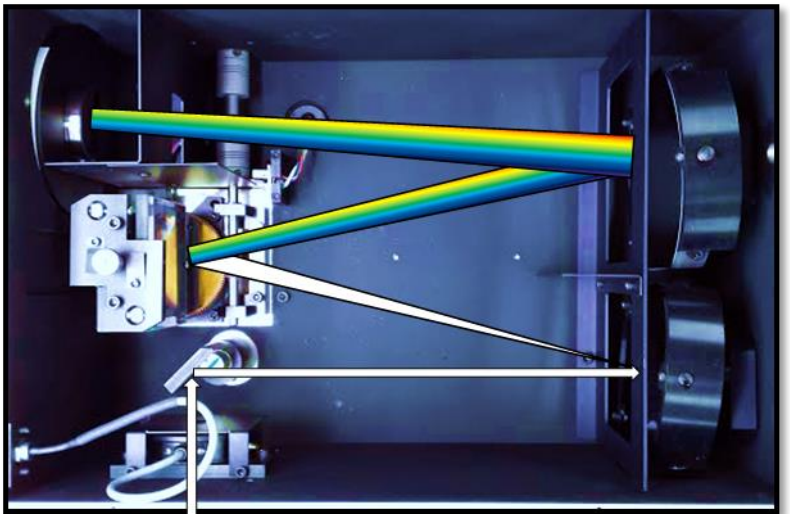

Figure 7 The inside of the spectrometer with the light path indicated. Light enters the spectrometer at the bottom of the diagram through a motorized slit which is set to a width of 100 micons. The light is then directed toward a grating via a focusing mirror, where it is diffracted into its constituent wavelengths. A second focusing mirror then focuses the light onto the CCD sensor, located in the upper left of the diagram.

The spectrometer is a Princeton Instruments ISO-160 in a Czerny-Turner configuration. The motorized slit is set to 100 microns for each of the experiments. The movable grating inside the spectrometer is angled so that light of wavelength 650 nm falls at the center of the CCD sensor. The camera is a Princeton Instruments PIXIS: 400BR eXcelon, thermoelectrically cooled to -70 °C. The sensor itself has a pixel width of 1340 pixels and a height of 400 pixels, with each pixel being 20 microns by 20 microns. The grating has a density of 150 grooves per millimeter and a Blaze wavelength of 800 nm. Combining this with the width of the sensor means that the wavelength range being collected is 268-1068 nm. For reference, the laser is 532 nm and the emission wavelength of the quantum dots is about 627 nm. An example of an image from the sensor is shown in Figure 8.

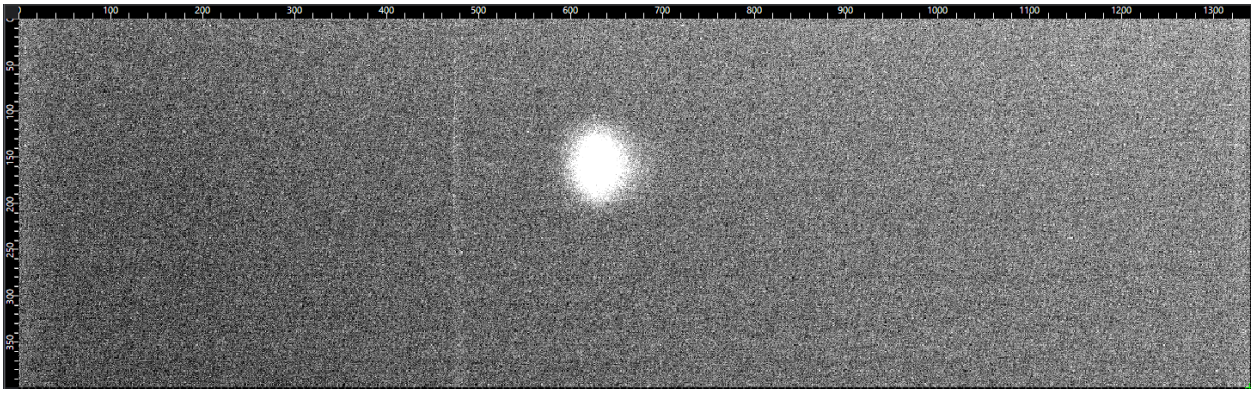

Figure 8 An image of the CCD sensor. The white spot near the center of the sensor is the light emitted by the quantum dots. The vertical line to the left of the white spot is the excitation light. This light has been drastically reduced by the filters but not eliminated. Note that the numbers at the top and left of the image are the pixel numbers, not the wavelength.

The exposure time for each frame is set to 500 milliseconds. For a standard photobrightening trial, the number of frames to be collected is 600. This means that the total time for each run is five minutes. A black background file is subtracted out to minimize the dark noise in the system. This dark noise has a value of about 600 counts and is intentionally introduced by Princeton Instruments in order to avoid possible negative intensity values. By subtracting out the dark noise, the image has a minimum value as close to zero as possible. There is a flip mount on which is mounted a beam block. This is controlled via remote and is activated simultaneously while starting a trial. When the trial ends, the beam block is moved back into place so as not to expose any other quantum dots while moving to a new region of interest. For each new region of interest, the sample is moved a minimum of 100 microns. This ensures that the excitation light from the previous region of interest has not interacted with the quantum dots of the new region of interest. Due to the fact that not every region of interest will have the same number of quantum dots, and that not all of the quantum dots will behave in exactly the same manner, there are certain qualifications that have been placed on the regions of interest during the data collection process.

The maximum value of the quantum dot emission, determined by the data cursor being placed at roughly the center of the signal region, must fall between 200 and 40000 counts. This ensures that the signal will be bright enough to be distinguished from noise and that while brightening, the quantum dot emission will not saturate the camera, which has a maximum value of 65535 (2^{16}-1) counts. Additionally, any trials where the quantum dots do not brighten are discarded, as brightening is the behavior in question.

Once the experimental run is completed, the data is exported as a series of .tiff files, one for each frame. While the Lightfield software used for the spectrometer has the capability to create frame cross-sections (a single line representing the average value of a selected region of the sensor for each frame), the results of using such a feature would not account for the differing numbers of quantum dots present in each region. This would skew the data to more heavily weight regions wherein the quantum dots took up a larger area of the sensor. To avoid this problem, the exported .tiff files are processed by a custom MATLAB code which determines the intensity and center wavelength of the quantum dot signals. The code can be found in its entirety in **Appendix B – MATLAB Code**.

The columns of each .tiff file are averaged together to form a single column. The greatest value row in that column is used as the target row, since it is the row most likely to be the vertical center of the quantum dot signal. The four rows above that target row and the four rows below the target row are then averaged together with the target row to create a new row of data. This new row has a slightly lower signal than the original but has a smoother signal. This averaged row is then fitted with a gaussian fit and the parameters are captured for use. The important parameters are the amplitude and x-offset of the gaussian. The amplitude gives the

intensity value and the x-offset, when calibrated against a wavelength conversion file thereby converting pixels to wavelength, gives the center wavelength. The process is repeated for each successive image. The intensity and wavelength values are then exported to Microsoft Excel. The remaining analysis of the data, both numerical and graphical, is performed in Excel.

CHAPTER III. QUANTUM DOT CHARACHTERIZATION

As a check against other papers, the quantum dots' initial photoluminescence as a function of laser power was determined and compared to a known data set. A single region of interest was studied at several different laser intensity levels. The optical density was varied from OD 0.0 to OD 3.0. The sample was exposed to the laser, a single frame was taken, then the laser was blocked. This process was repeated for each of the laser intensity values. Once the process was completed, another region was chosen. After five trials, the order of the intensity was reversed, so rather than start with the highest intensity, the experiment started with the lowest. Five more trials were conducted. The data is shown in Figure 9 on a log-log scale. Next to it is data taken from [37]. The data taken clearly shows the same trend as the data from [37].

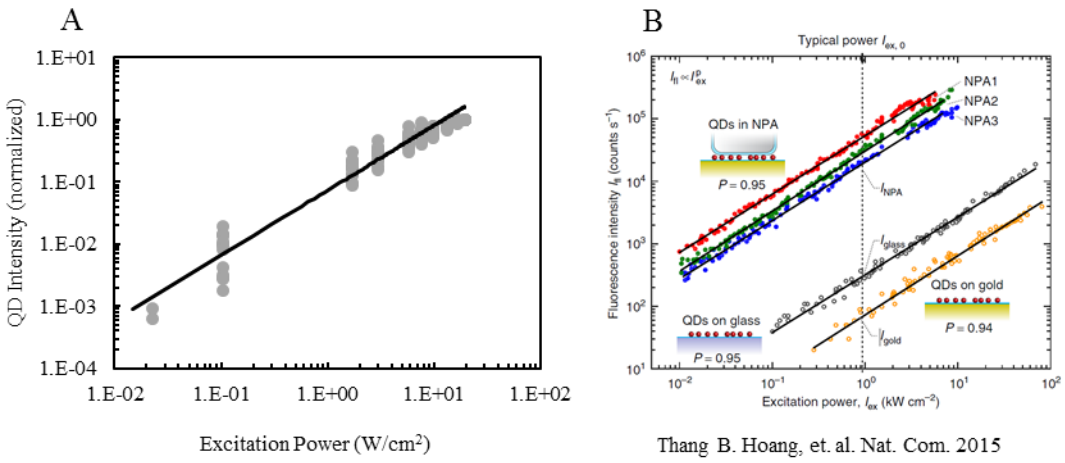

Figure 9 (A) shows the initial value of the quantum dots as the excitation intensity is changed. The data has been normalized to the maximum value as not every region of interest will have the same initial brightness. (B) shows the data taken from [37] whereby the initial intensity of quantum dots was studied under various laser intensities and differing surrounding conditions. The quantum dots in (A) are on silicon with no other nanoparticles present, making the data most closely resemble the grey line labeled I_{glass}.

As the quantum dots are exposed to the laser, the photoluminescence signal increases over time. An example for the quantum dots used here is shown in Figure 10.

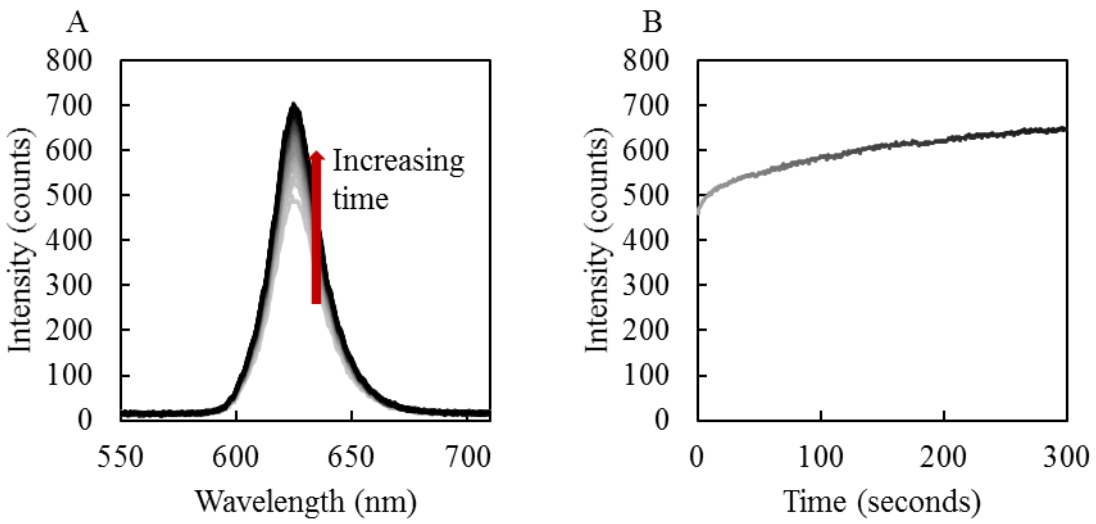

Figure 10 (A) The evolution of a quantum dot spectrum over time. The darker lines represent later times, illustrating the photobrightening that takes place under continuous excitation. (B) The peak intensity change over time. The shade changes along with the time as in (A).

The change in intensity shown in Figure 10 is for one region of interest. However, as noted before, each region of interest will have a different base intensity depending on the number of quantum dots in the region, as each quantum dot will contribute to the intensity and can photobrighten. This means that simply taking the average intensity before and after exposure will give an inaccurate picture, weighted sharply toward the brightest regions. Instead, the relevant parameter is the percent change in the intensity. The percent change is calculated for each region individually, then the results are averaged together. This is illustrated in Figure 11.

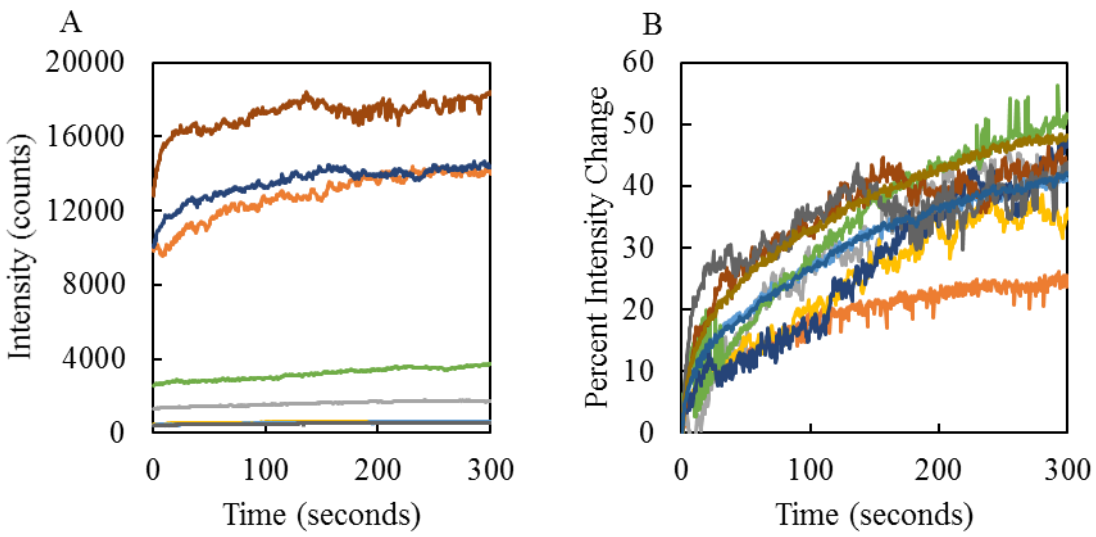

Figure 11 (A) A graph of the intensities over time for several regions of interest with each color representing a different region of interest. The values vary from a few hundred counts to nearly 20000 counts. (B) The same regions of interest, plotted as a percent change of the original value, but unchanged in the colors. Each of these used the same laser intensity of 1.74 W/cm^2. Note that there is no correlation between the initial value of the trial and the percent change.

As shown in Figure 11, there is a wide variation between the initial intensities for the various regions, a difference which is well-repeated in each different photobrightening experimental trial conducted. Clearly illustrated is the fact that there is not correlation between the initial brightness and the percent change, most easily shown by the fact that the region represented by the orange line is the third brightest in initial intensity but photobrightens the least while the regions represented by the brown and green lines, lines which are significantly above (brown) and below (green) the orange line photobrighten significantly more. A more accurate picture can be obtained by the normalization process outlined above. This creates significantly more closely grouped data. The data in Figure 11 can now be replaced by an average of the intensity values, shown in Figure 12.

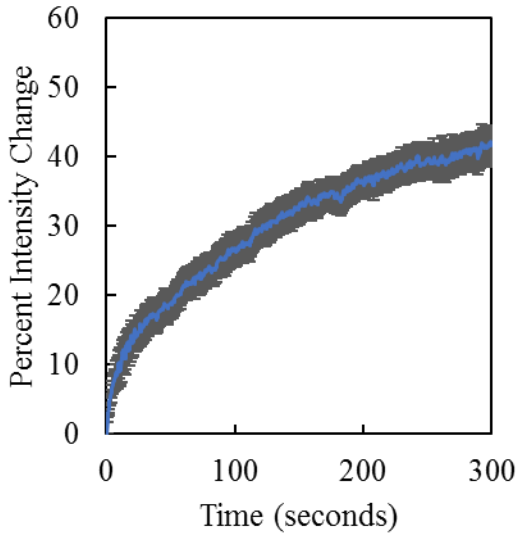

Figure 12 The average of the percent change of several regions of interest. The grey surrounding the blue line is the sampling error

As has now been shown, this creates a tighter sampling group. The percent change is roughly the same between regions of interest. The next question is whether the photobrightening depends on the intensity of the excitation light in the same way that the initial intensity does, a question not previously answered. To that end, a sample of pure quantum dots on a silicon substrate was tested repeatedly under various laser intensities. Each laser intensity was used to illuminate ten different regions of interest for 600 seconds a piece. The laser intensities were 0.11, 1.74, 2.99, and 5.86 W/cm^2. These represent the use of optical density values of 2.0, 1.0, 0.8, and 0.5 respectively. The results are shown in Figure 13.

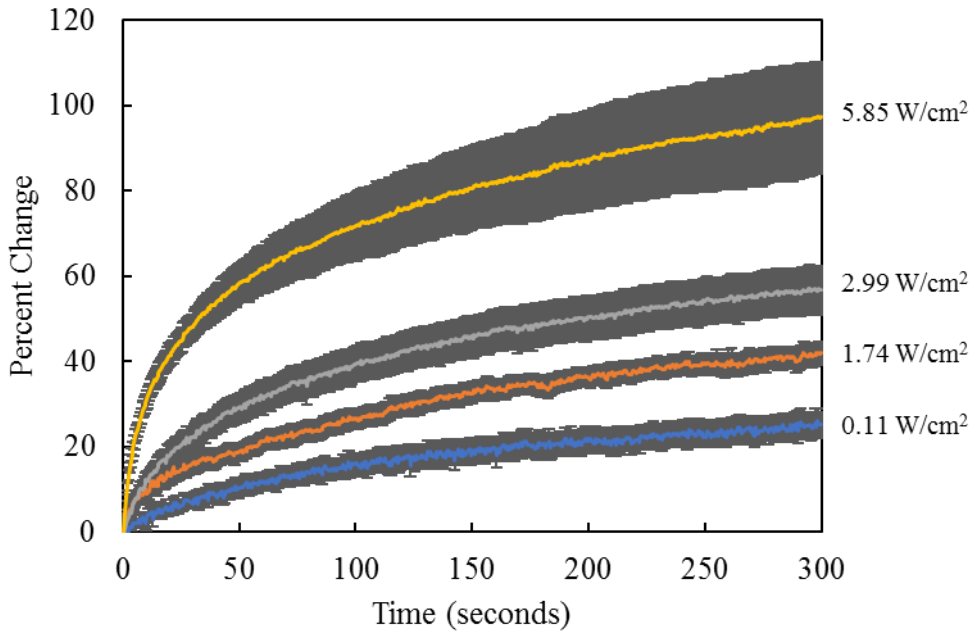

Figure 13 The percent change in the intensity of quantum dots under various laser intensities. The dark grey surrounding each line is the standard error. Noted to the side of each line is the laser intensity at the substrate.

Figure 13 clearly shows that an increase of laser power leads to an increased photobrightening. This is expected as the photobrightening is likely caused by either photo-induced passivation or thermal-induced phonon effects, either of which would be increased with an increased excitation intensity. The increase becomes even more apparent when the percent increase after 600 seconds is plotted against the excitation intensity, as shown in Figure 14.

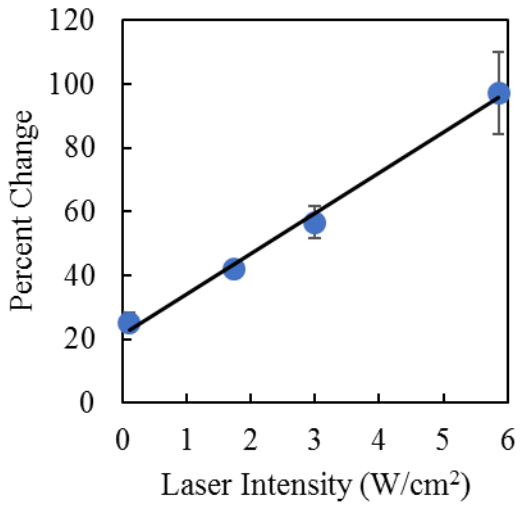

Figure 14 The photobrightening after 600 seconds is shown as a function of the laser intensity at the substrate.

The linear relationship between the photobrightening and excitation energy is clear. The reason for the lack of continued data is due to limitations of the equipment. The CCD camera of the spectrometer has a maximum value of 65535. Increased excitation intensity leads to photobrightening beyond the measurable values of the camera. The linearity of the relationship between the percent change of the intensity after 600 seconds and the excitation intensity likely means that there is a much higher threshold for saturation of the quantum dots, as an unbounded increase is decidedly non-physical. However, for photobrightening rates around those given here, the linear scaling means that it is significantly easier to predict the excitation intensity given a photobrightening value. There is, of course, also no reason that the quantum dots should photobrighten at all with an intensity of zero, as indicated by the graph. The reason for the lack of data in that area is a detection limit. There is too low a signal-to-noise ratio to be able to detect photobrightening with a lower laser intensity. A note of some import is due here – the linear relation present is likely in all quantum dots which are able to photobrighten at approximately the

rates here given, but the slope of the graph, and of course the values within, will change between fabrications of quantum dots, as well as with the age of the quantum dots. It would therefore be essential to repeat the measurements given here prior to using this data for any meaningful characterization.

CHAPTER IV. COMPUTATIONAL PLASMONIC EFFECTS

i. Single Particle Response

Having determined the effect that laser intensity has on photobrightening, plasmonic nanoparticles can now be added to determine if the plasmonic enhancement will have an effect on photobrightening. Several nanoparticle sizes were procured from nanoComposix. These gold nanospheres have diameters of 60, 80, and 100 nm. The relevant parameters for these particles from a plasmonic enhancement perspective are the scattering and absorption spectra. As these are solid gold nanospheres, Mie theory can be used to compute the scattering and absorption profiles for individual particles. Algorithms developed by Bohren and Huffman[56] were distilled into a MATLAB code by Matzler[57]. This code had to be modified to function properly, but after some modifications it could be used to predict the absorption and scattering profiles for gold nanospheres. Using this code, along with refractive index data taken from Johnson and Christy[58], the scattering and absorption spectra were computed and are shown in Figure 15.

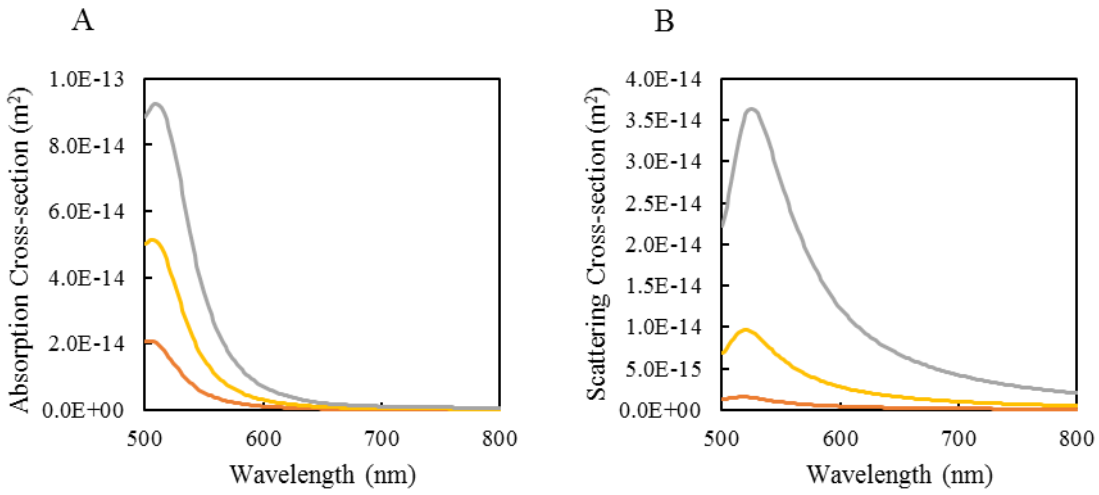

Figure 15 (A) Absorption and (B) scattering spectra in arbitrary units as calculated by MATLAB code for individual particles. The colors represent the same size particles for each graph.

This spectrum is the result of solving differential equations set forth by Bohren and Huffman prior to computational electromagnetics being commonplace. As a check on the accuracy of the code, the finite-element method computational physics program COMSOL was used to make the same calculations, using an initial electric field of 1 V/m, polarized in the x-direction. The results are below in Figure 16.

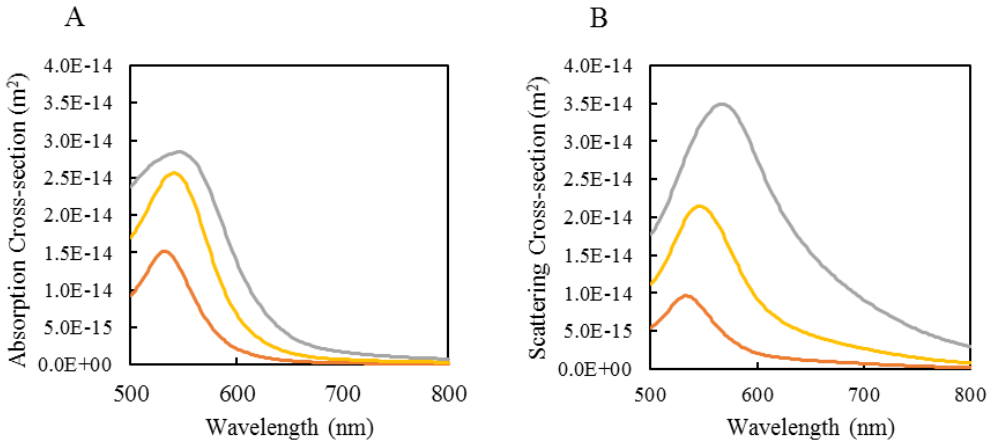

Figure 16 (A) Absorption and (B) scattering spectra in arbitrary units as calculated by COMSOL simulations for an individual particle.

As is clear from the figure, there is a difference in the amplitude of the spectra depending on the method of calculation, but the peaks are in the same place. The COMSOL model also gives a good opportunity to visualize the electric field of a nanoparticle. The model used is a single gold sphere suspended in water. For simplicity, water is assumed to have a refractive index of 1.33 across all wavelengths. The solved model, illustrating the electric field and charge distribution, is shown in Figure 17.

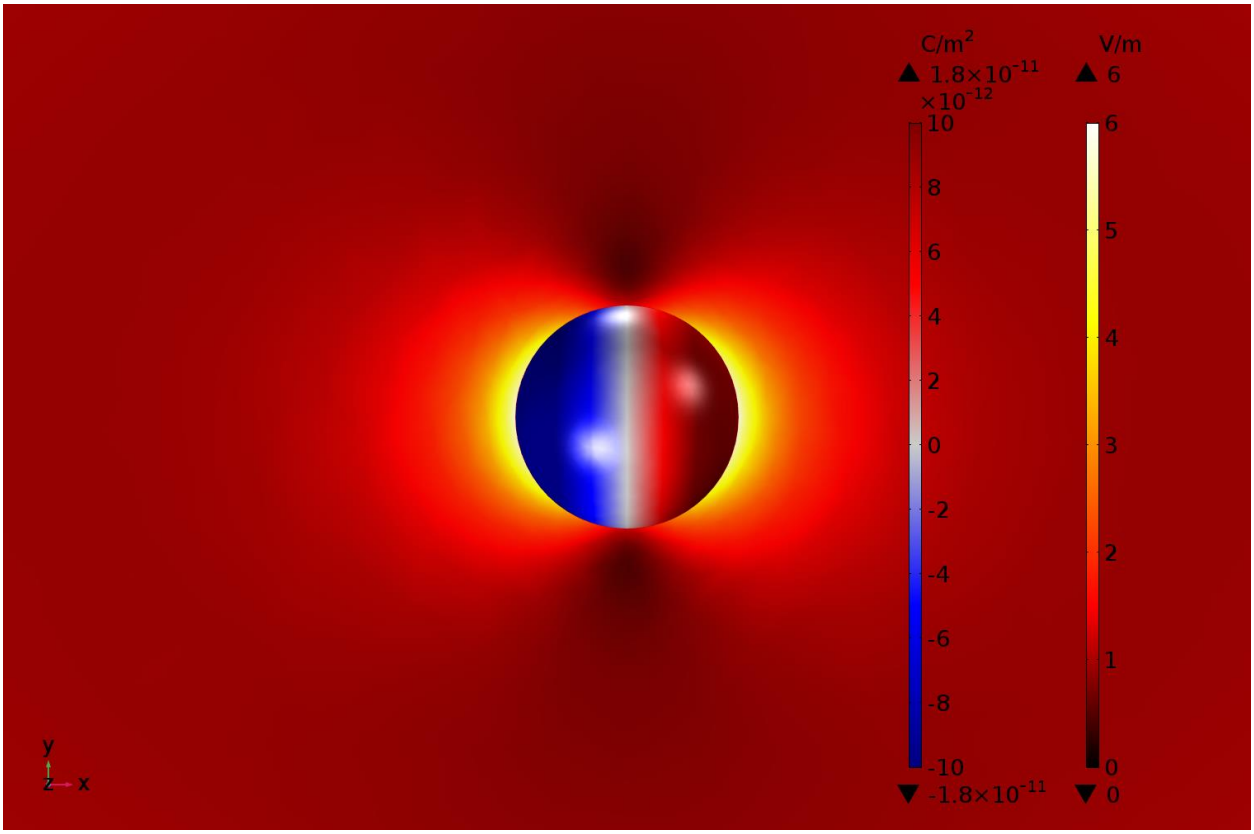

Figure 17 The electric field distribution and resultant electric field when a 100 nm diameter gold nanosphere is illuminated with a 532 nm wavelength 1 V/m electric field polarized in the x-direction and propagating in the negative z-direction. The surface of the sphere is color-coded to display the charge distribution in C/m^2 with red being a positive charge and blue being a negative charge. The area outside of the sphere shows the strength of the electric field. Though the electric field is in units of V/m, the incident field has a strength of 1 V/m, meaning that the values displayed are also the relative strength of the field.

Figure 17 gives the electric charge distribution on the surface of a 100 nm diameter gold nanoparticle. The incident electric field is in the negative z-direction (into the plane of the image) and polarized in the x-direction. The result of the electric field interacting with the gold sphere is that the charge distribution forms a dipole in the direction of the polarization. This dipole then serves to create its own electric field, shown by the background of the image. There is a very strong field surrounding the surface of the nanoparticle, strongest closest to the greatest charge density. The electric field far from the surface returns to a value of 1 V/m, identical to that of the

initial field. Additionally, at the top and bottom of the sphere the field is less than that of the initial field. This illustrates the defining feature of plasmonic enhancement. The field close to the particle can be enhanced, and in this image there is an enhancement of the electric field of almost a factor of 6, but the total field is not enhanced, rather, the field strength has been redistributed around the sphere to match the magnitude of the charge distribution. Far from the sphere, where the electric field has returned to a value identical to the initial field, there has been no change in the field, meaning that a probe which is looking at far-field light, such as the optical microscope used in this paper, will see little to no change in the light. In fact, due to non-radiative losses, the total field is reduced by a small amount[59]–[61].

Next the absorption and scattering for the quantum dots are to be calculated using COMSOL. Simulating the quantum dots uses a two-layer sphere with a CdSe core of 3 nm and a CdS shell with a 2 nm thickness. Data for CdSe[62] and CdS[63] were taken from Ninomiya and Adachi. The absorption is calculated using an integration sphere a short distance from the surface of the sphere (2 nm) and the scattering is calculated at the interior surface of the outer wall of the simulation space. There is a problem, however, when trying to calculate the spectra for the quantum dots; classical electrodynamics does not function well below a certain particle size for a single particle due to quantum restrictions. The minimum size for a single particle for optical wavelength simulations is approximately 40 nm. Below this size, COMSOL has problems with the simulation due to these quantum limitations. This problem is obvious when observing the calculated scattering spectrum for the quantum dots, as shown in Figure 18.

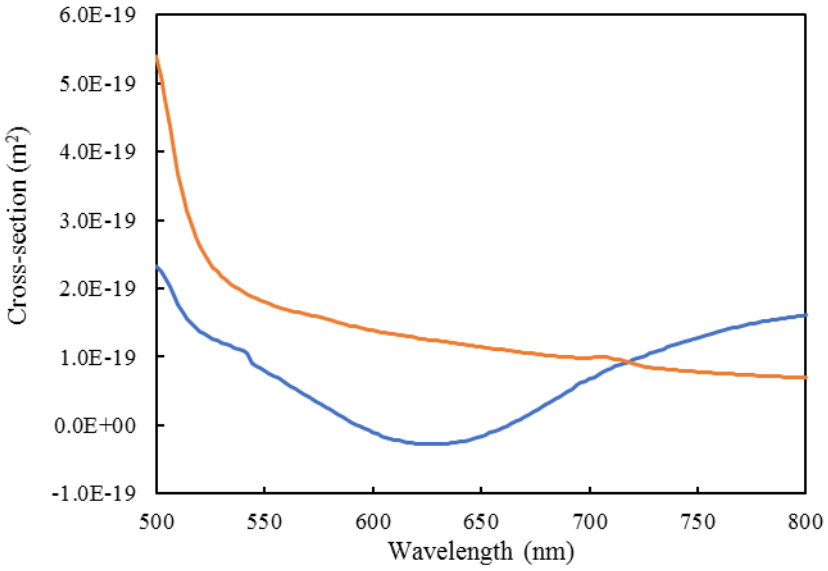

Figure 18 The scattering (blue) and absorption (orange) spectra of a quantum dot as simulated by COMSOL, in arbitrary units. An obvious problem with the spectra is that the scattering spectrum dips below the zero mark, indicating a (physically impossible) negative scattering value.

The problem shown in Figure 18 is a limitation of COMSOL, but only poses a problem when there is only one sphere present. It is also only an issue when determining the scattering spectrum. The minimum value of the scattering cross-section, however, does occur at the emission wavelength of 627 nm, showing that the negative scattering cross-section results in the emission, as discussed in [64].

One of the major advantages to COMSOL is the ability to compute the electric field for a given situation. For a quantum dot being excited by an external field, the important factor is the electric field at the surface of the quantum dot. Making the assumption that the most important wavelength is the excitation wavelength, rather than the emission wavelength, the remaining simulations will be conducted at a wavelength of 532 nm. By integrating the electric field over the surface of the quantum dot, a baseline field without the plasmonic enhancement can be

established. Integrating the function *emw.normE* (the magnitude of the electric field) over the surface of the quantum dot and then dividing by the surface area gives a value of 0.776 V/m. This will be the value used to determine the enhancement of the light at the surface of the quantum dot. This value is independent of the direction of the incoming light, as is appropriate, given the spherically symmetric nature of the simulation.

ii. Dual Particle Response

Base response established, the simulation can now be modified to include a gold nanosphere. The method of determining the absorption means that the integration sphere needs to be placed at the center of the simulation. To keep the positioning of the sphere, the nanoparticle and quantum dot are offset from the center. The gap between the quantum dot and the nanosphere is set to 2 nm, approximately the length of one of the ligands. The newly non-symmetric nature of the simulation means that the position of the quantum dot relative to the nanoparticle will matter. To that end, simulations were run altering the angle between the quantum dot and the nanoparticle, relative to the polarization vector, from 0° to 90°. At an angle of 0° the quantum dot is in the strongest electric field. At an angle of 90° the quantum dot is in a region of the electric field which has a strength less than the incident field. An example of this is illustrated with a 100 nm sphere in Figure 19.

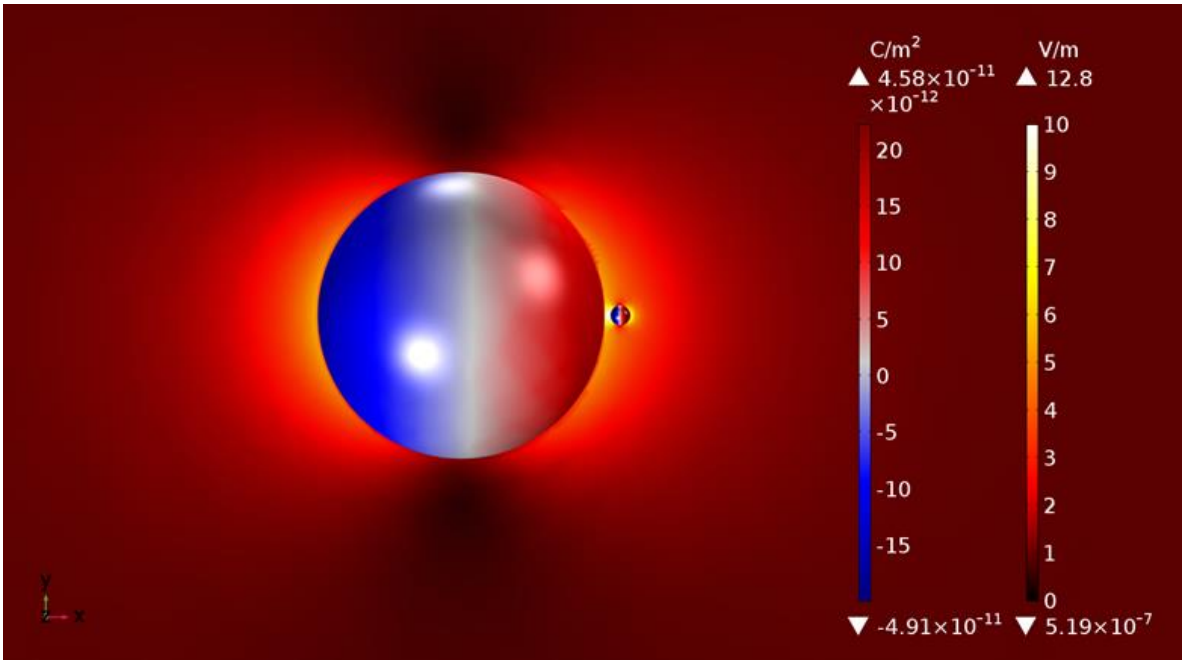

Figure 19 The electric field and charge distribution for a quantum dot next to a 100 nm diameter gold nanosphere. The large central sphere is the gold nanoparticle and the smaller sphere is the quantum dot. The red and blue on each sphere is the charge distribution and the background of the image shows the electric field. The quantum dot is at an angle of 0° from the nanoparticle with respect to the polarization vector, putting it in the strongest region of the electric field. An enlarged image of the quantum dot is shown in the inset, highlighting the large electric field and strong dipole moment.

From the above figure, it is clear that there is a significant dipole moment, both in the gold nanosphere, central to the image, and in the smaller quantum dot off to the side. By placing the quantum dot in line with the polarization vector with respect to the nanosphere, the electric field surrounding the quantum dot is at its highest, leading to greater photobrightening. Integrating the electric field at the surface of the quantum dot, and dividing by the surface area, gives a value of 1.808 V/m, representing an enhancement factor of 2.33 over the electric field at the surface of the quantum dot without a nanoparticle present. As the optical intensity is proportional to the square of the electric field, this gives an optical enhancement factor of 5.43. This enhancement factor is, however, only valid for the quantum dot being in line with the polarization vector and nanosphere.

When placed perpendicular to the polarization vector the situation changes drastically, as shown in Figure 20.

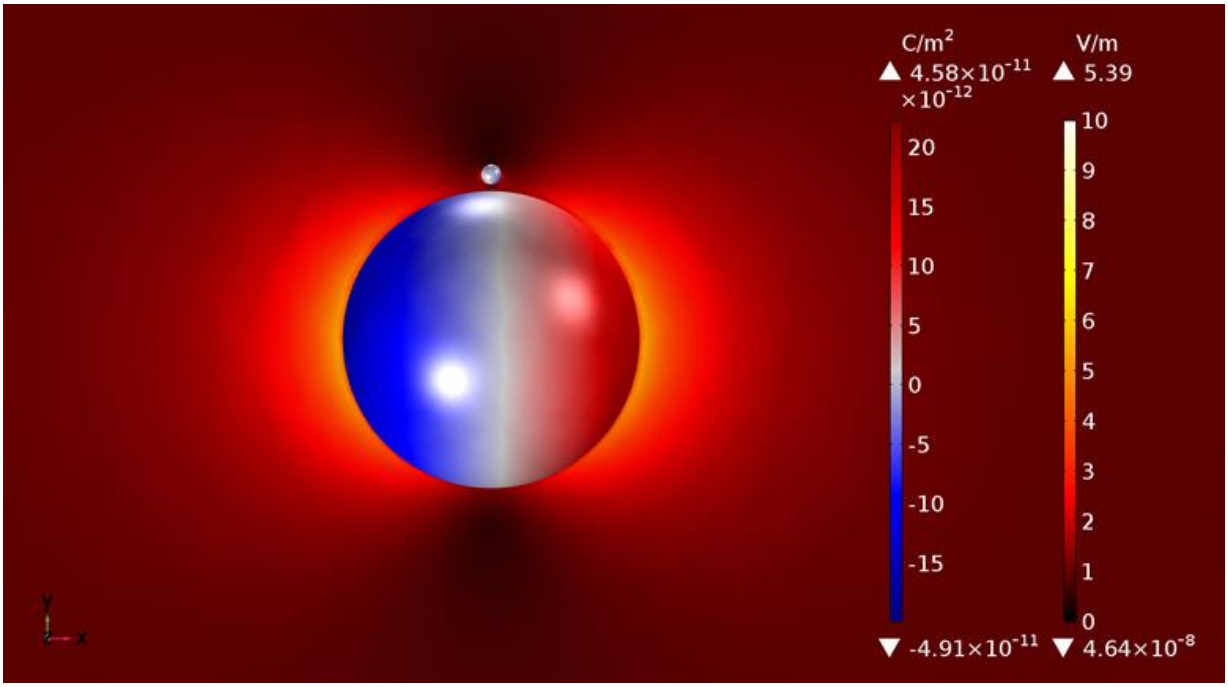

Figure 20 The electric field and charge distribution for a quantum dot next to a 100 nm diameter gold nanosphere. The large central sphere is the gold nanoparticle and the smaller sphere is the quantum dot. The red and blue on each sphere is the charge distribution and the background of the image shows the electric field, a scale which is the same as in **Figure 19**. The quantum dot is at an angle of 90° from the nanoparticle with respect to the polarization vector, putting it in a region of the electric field with a value below the background. An enlarged image of the quantum dot is shown in the inset, highlighting the low electric field and illustrating the quadrupole electric charge distribution.

Moving the location of the quantum dot leads to a very different set of outcomes, chief among which is the alteration of the charge distribution of the quantum dot. The charge distribution of the nanoparticle is largely unchanged while the quantum dot now displays a quadrupole moment rather than a dipole. The moment is also significantly weaker than before. Integrating the field at the surface of the quantum dot and dividing by the area gives a field of 0.306 V/m, representing an electric field enhancement of 0.395, and an optical enhancement factor

of 0.156. This is a decrease in the light which is exciting the quantum dot, leading to a lesser amount of photobrightening. The consequence of this is that even discounting the quenching which can result from quantum dots in close proximity to metallic nanoparticles, the decrease in the field in certain areas can still result in damped photobrightening over the case with no plasmonic enhancement. The enhancement factor is cyclical as the angle moves from 0° to 360°; a graph illustrating the change from 0° to 90° is shown in Figure 21.

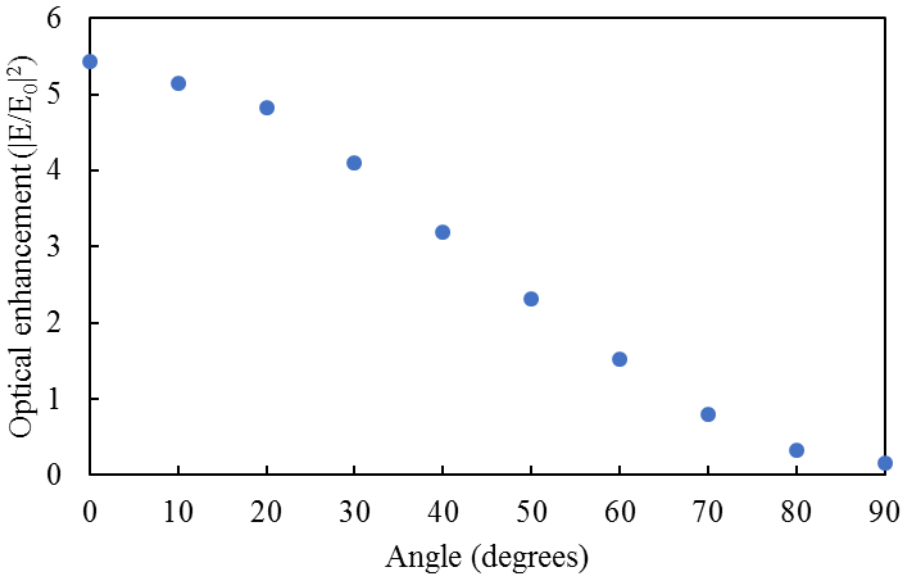

Figure 21 The optical enhancement at the surface of the quantum dot as determined by the square of the ratio of the electric field at the surface of the quantum dot with plasmonic enhancement to the same quantity without plasmonic enhancement. For 70°, 80°, and 90°, the optical enhancement factor is below 1, representing a decrease in the excitation light, and therefore a decrease in the photobrightening.

By changing the angle, there is a sharp drop in the optical enhancement factor of the excitation light, causing the photobrightening to be damped by a significant amount. Additionally, as the quantum dot is moved around the nanoparticle the dipole moment is rotated as well. Until such a point as the quadrupole becomes the dominant multipole moment, the dipole moment is

perpendicular to the nanosphere. While this phenomenon is not the focus of this dissertation, it does lead to the idea that a polarizer between the sample and the camera would allow for the determination of the orientation of the quantum dot with respect to the nanosphere. There is no physical reason why the quantum dot would be at a certain angle with respect to the nanoparticle, meaning that no enhancement factor should be more likely than any other, leading to the need of an average enhancement factor. For the 100 nm sphere, assuming that the quantum dot is 2 nm from the surface, the average enhancement factor of 532 nm light is 2.78. Conducting the same trial for the 30 nm and 40 nm spheres leads to similar behavior. This is summarized in Figure 22.

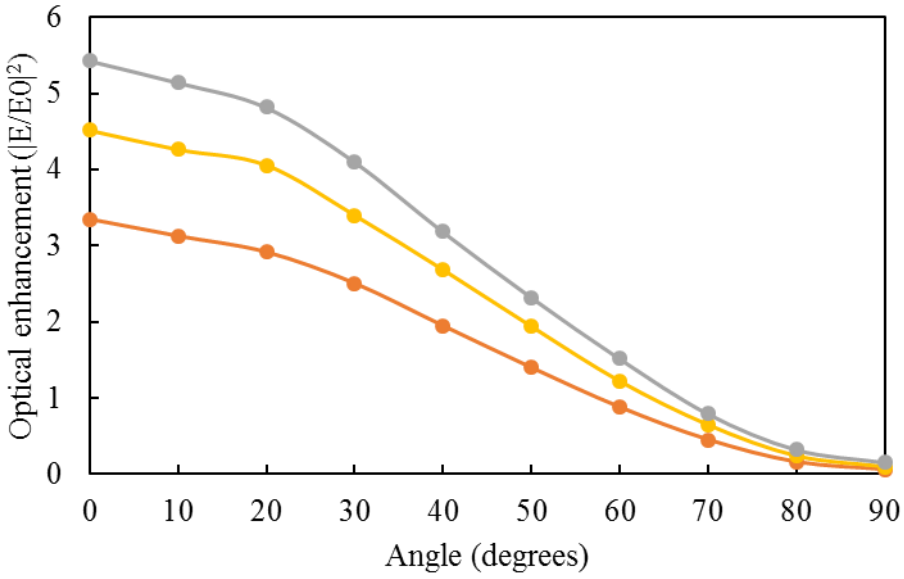

Figure 22 The optical enhancement factor for each of the three sizes of spheres at various angles. Note that all follow the same trend and each, at certain angles, has values below 1.

As expected from the simulations of the nanoparticles by themselves, there is a sharp distinction between the enhancement factors based on the size of the nanoparticle paired with the quantum dot. The size of the nanoparticle also determines the angle at which the enhancement factor dips below 1, or the angle at which the photobrightening will begin to be damped. The wide

variety of optical enhancement factors means that, while on average there will be an enhancement of the photobrightening, there is also likely to be a wide range of photobrightening values and means that an experiment which shows a photobrightening which is less than the photobrightening of pure quantum dots is not, ipso facto, a refutation of the idea of plasmonically enhanced photobrightening. Indeed, it is almost to be expected. The lack of increased photobrightening, however, does not indicate prima facia that the photobrightening will be stopped. It remains, therefore, appropriate to discard photobrightening trials which do not show photobrightening, or, indeed, show photobleaching, as photobrightening is the focus of this dissertation.

CHAPTER V. EXPERIMENTAL PLASMONIC EFFECTS

i. Nanospheres

Armed now with the insight gained from the simulation, it is time to attend to the experimental verification. The same photobrightening experiments performed without nanoparticles were then performed with them. To minimize the time-dependent effects which are on the scale of days or weeks[25], the photobrightening experiments with nanoparticles were performed at the same time as those without them. With the addition of the nanoparticles, the photobrightening is changed. Contrary to the report by Chen[54], the photobrightening is not quenched. Instead, as hypothesized, it is increased. Taking, as an example, the comparison between a sample without nanospheres and a sample which includes 100 nm gold nanospheres, with a laser intensity of 1.74 W/cm^2 there is a 42% increase in the intensity without nanoparticles and a 158% increase in the intensity with the addition of nanoparticles, giving an enhancement factor of 3.76. This is illustrated in Figure 23.

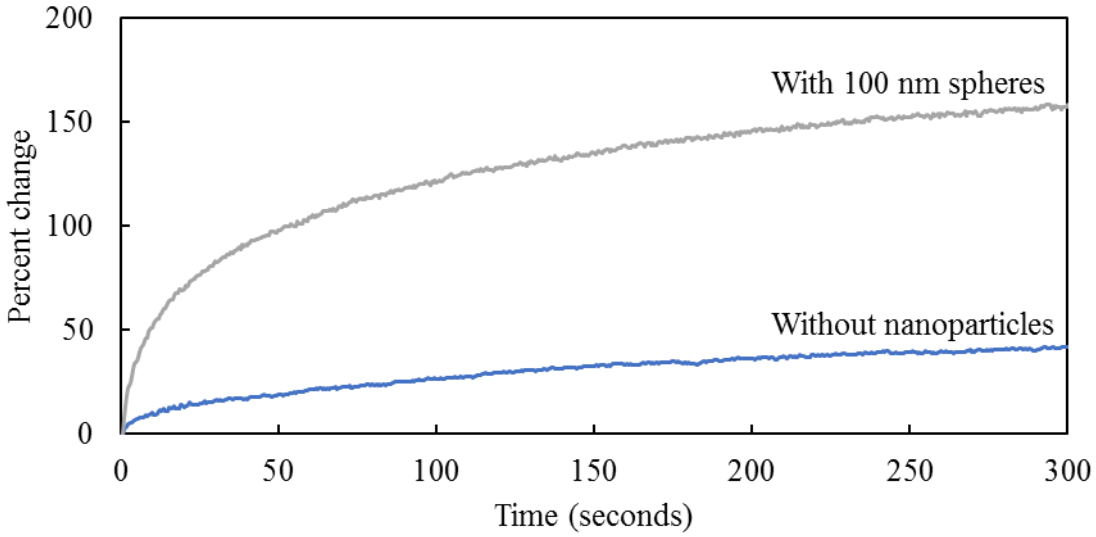

Figure 23 Photobrightening effects by the addition of 100 nm spheres. The blue line represents quantum dots with no nanoparticles and the grey line shows the intensity change with the plasmonic particles added. Each of these results are the average of ten separate regions of interest.

The figure clearly shows a dramatic increase in the rate of photobrightening. It should be again reiterated that this does not represent an increase necessarily in the intensity, as each region studied will have different numbers of quantum dots and hence a differing initial intensity, merely an increase in the amount by which the initial intensity in each region has changed. This increase is not as dramatic with the use of other particles, but still present. More importantly, there is no case tested in which the addition of nanoparticles caused the percent change in the photobrightening to be diminished from the case wherein there were no nanoparticles added, reflecting the idea presented in the simulations that the average enhancement value for each of the types of nanoparticles is above 1. The nanoparticles that were used were suspended in deionized water. Each of the samples had the same mass density of 0.05 g/mL. The absorbance spectra for each of the samples was measured in suspension and the results are shown in Figure 24.

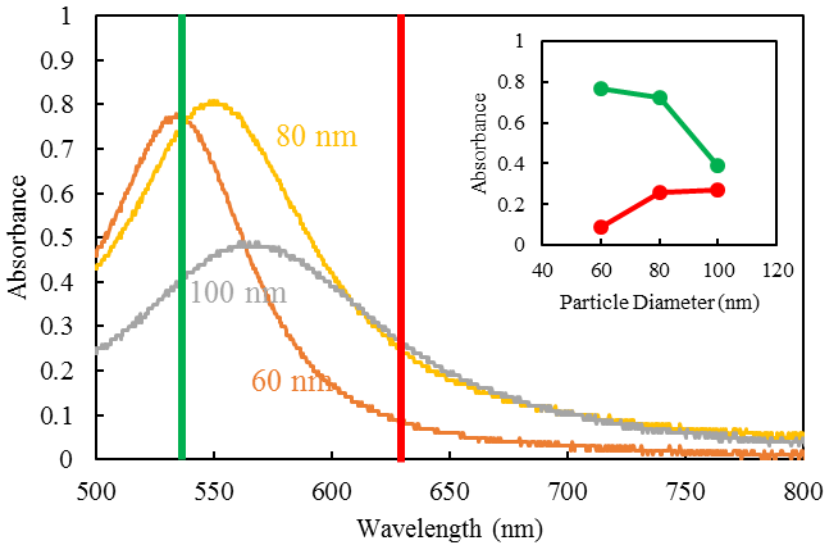

Figure 24 The absorbance spectra for each of the nanoparticle samples. The samples are suspended in deionized water at a mass concentration of 0.05 g/mL. The spectral lines for excitation and emission are marked with green and red lines respectively. The values for the absorbance at each of the marked wavelengths for each of the particles are shown in the inset.

The absorbance spectra are similar, although not identical, to the absorption spectra calculated in MATLAB and simulated in COMSOL. There is a difference in the amplitudes as well as the location of the peaks; both of these factors are due to the fact that there is not a single nanoparticle being analyzed, rather it is an ensemble[65]. As these are experimental measurements of the particle solution being used, rather than computational effects of a single particle, these data are the ones which will be used throughout the experimental portion of this work. Photobrightening experiments were conducted using 60 nm, 80 nm, and 100 nm gold nanospheres. Ten different regions of interest were tested for each of the samples and three different laser intensities were used. The results of the experiment are shown in Figure 25.

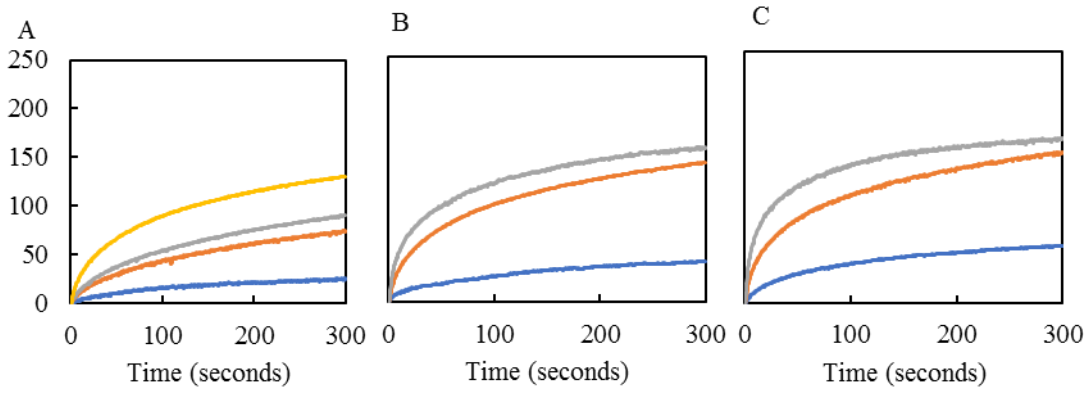

Figure 25 The photobrightening changes for quantum dots combined with each of the three types of nanoparticles. The three different laser powers are (A) 0.105 W/cm^2, (B) 1.74 W/cm^2, and (C) 2.99 W/cm^2. The different samples are indicated by the different colored lines – 60 nm in orange, 80 nm in yellow, and 100 nm in grey, with the unenhanced quantum dots in blue.

The graphs make it clear that the nanoparticles provide a significant enhancement to the photobrightening. Also clear is that there is a significant dependence on the size of the nanoparticles. Like the unenhanced quantum dots, each plasmonically enhanced sample has an increase in the photobrightening with increased laser intensity. The line for the 80 nm spheres is

present only in one graph. This is due to technical limitations of the system. The trials for the 80 nm particles brightened the system significantly more than the others. This pushed the intensities for the later times past the saturation level for the camera, thus they were not able to be included.

The nanoparticle solutions were initially tested with identical mass concentrations. However, due to the fact that different sized nanospheres require different amounts of gold, the nanoparticle samples contain differing numbers of particles. While the location of the peaks are dependent upon the size of the particles, the amplitude of those peaks are determined by the number of particles, not the total amount of material. To get a better idea of the enhancement factors for each of the particles, the solutions were diluted to a value of 5×10^9 particles/mL. As this changes the amplitudes of the spectra, a new absorbance profile was measured; the results are shown in Figure 26.

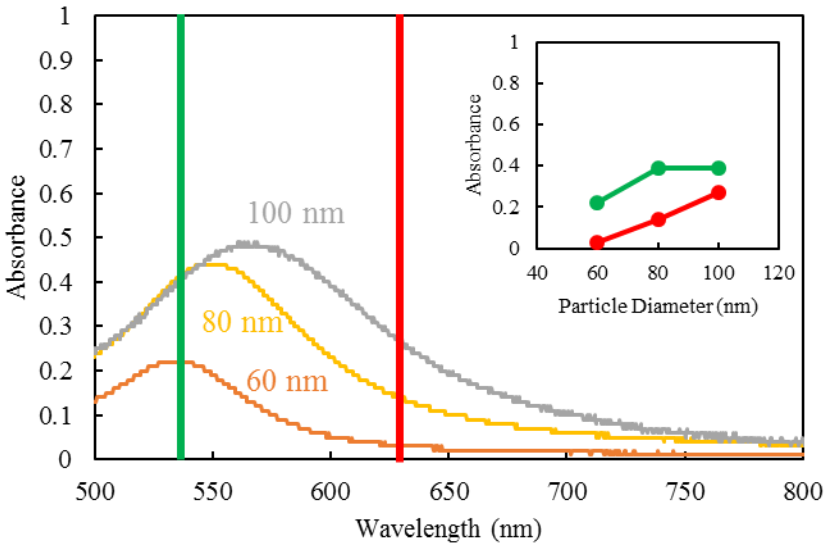

Figure 26 The absorbance spectra for the diluted nanoparticles. The spectral lines for excitation and emission are marked with green and red lines respectively. The values for the absorbance at each of the marked wavelengths for each of the particles are shown in the inset with the absorbance at the excitation wavelength in green and the absorbance at the emission wavelength in red.

There is a significant decrease in the amplitude of the spectra with the decrease in particle concentration. This decrease in particles should also lead to a decrease in the enhancement of the photobrightening. To test this, the previous photobrightening experiments were run using the diluted nanoparticles. The results of the trials are shown in Figure 27.

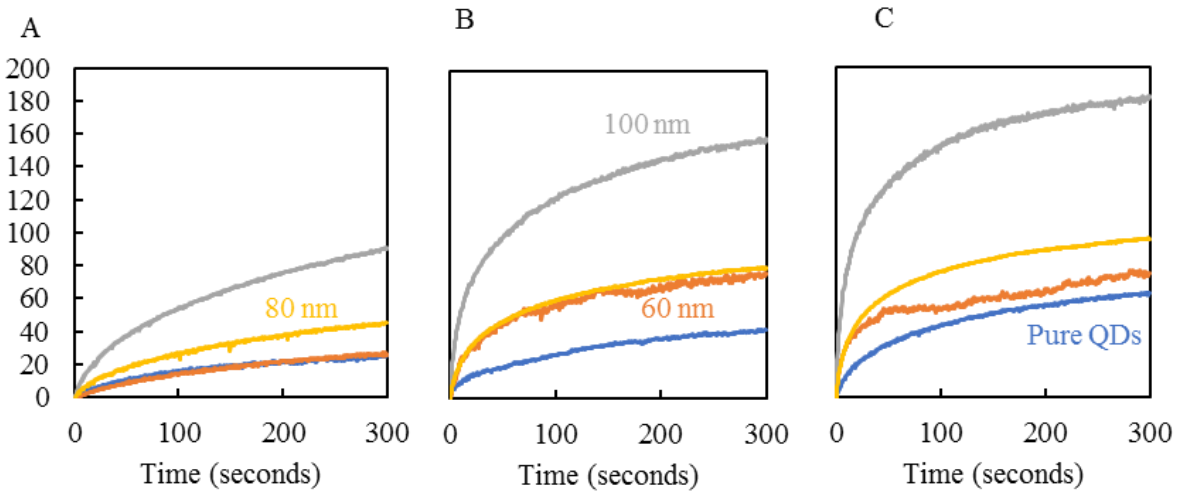

Figure 27 The photobrightening changes for quantum dots combined with each of the three types of nanoparticles after dilution. The three different laser powers are (A) 0.105 W/cm^2, (B) 1.74 W/cm^2, and (C) 2.99 W/cm^2. The different samples are indicated by the different colored lines – 60 nm in orange, 80 nm in yellow, and 100 nm in grey, with the unenhanced quantum dots in blue. Each of the nanoparticle samples has been diluted to the same particle concentration of 5×10^9 particles/mL.

The sharp decrease between the photobrightening values of the undiluted and diluted nanoparticle trials makes clear that there is a dependence on the number of particles. As the absorbance of the particles is not linearly dependent on the size of the particles, the photobrightening percentage at 600 seconds was plotted against the absorbance at both the excitation and emission wavelengths for each of the particle concentrations tested. The data is shown in Figure 28.

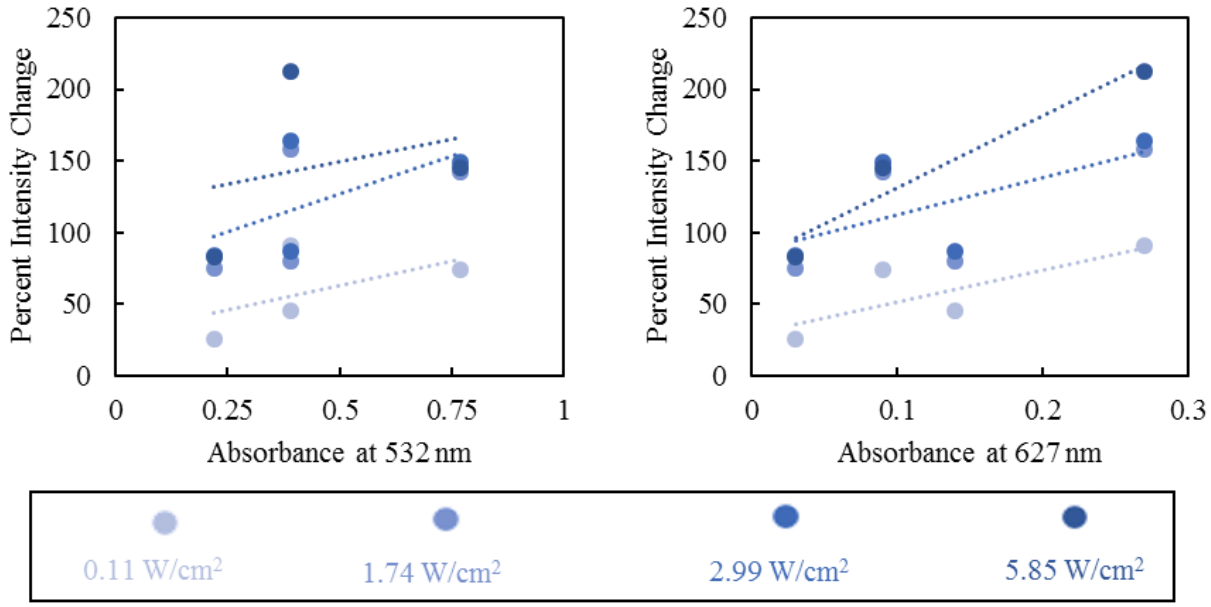

Figure 28 The correlation between absorbance for (A) 532 nm and (B) 627 nm and the photobrightening at 600 seconds. The darker data points have a greater excitation intensity.

Based on the data, there is some correlation between the absorbance at 627 nm and the percent intensity change. This correlation is significantly weaker for the absorbance at 532. With 532 nm being the excitation wavelength and 627 being the emission wavelength, this suggests that if it is a thermal effect, the heating occurs by the nanoparticles absorbing the emitted light, which might otherwise be wasted, causing the phonon contributions when the energy from the nanoparticles is fed back to the quantum dots. However, this is the same mechanism as is used for quantum dot quenching, that is, Förster resonance energy transfer[54], [66]–[68]. Förster resonance energy transfer, or FRET, is the process by which a donor particle allows energy to be transferred to an acceptor. The overlap between the emission spectrum of the donor and the absorption spectrum of the acceptor determines the efficiency of the transfer. By donating energy to the nanoparticle, the quantum dot has less energy with which to emit light, causing quenching. This means that while there is a correlation between the variables, it is not likely the cause.

Furthermore, absorption itself is unlikely to be the cause as the absorption at 532 nm, which could easily create phonon contributions without causing Förster resonance energy transfer, has a very weak correlation.

The weak correlation between absorption and photobrightening means that there is unlikely to be a thermal effect driving photobrightening, pushing the explanation more toward an optical effect. The relevant parameter to increase an optical effect is the scattering profile. Per the nanoComposix website, who supplied the particles, the scattering profiles for the various nanospheres used is given in Figure 29.

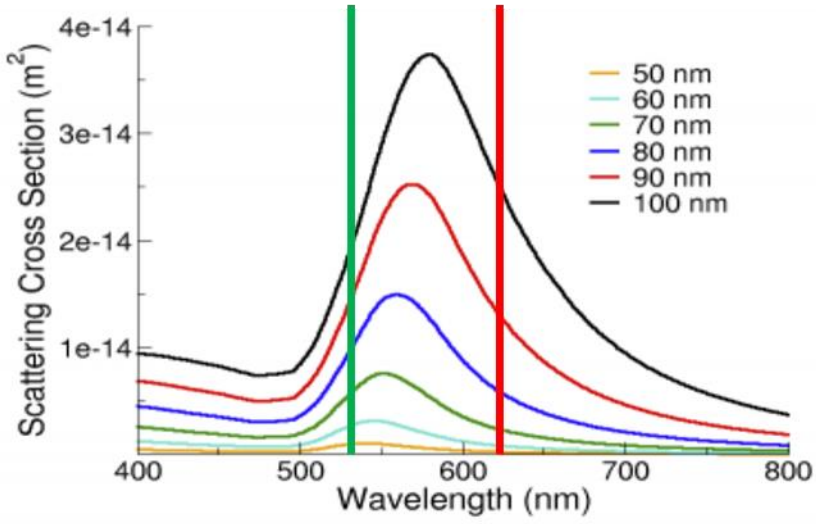

Figure 29 Scattering cross-section of gold nanospheres. The vertical green and red lines show the excitation and emission wavelengths, respectively. Image courtesy of nanoComposix.com

The scattering spectrum in Figure 29 gives the scattering cross-section of an individual nanoparticle. The data is measured with the nanoparticles suspended in deionized water and the cross-section is then determined by use of the Beer-Lambert law. Like the absorbance measurements, the scattering cross-section here presented is not the same as the calculated values from COMSOL or MATLAB. Again, as these are experimental values from an ensemble, these

are the data which will be used for this work. While it is not accurate to say that a single nanoparticle cross-section is the relevant parameter, as there is the distinct possibility, and indeed probability, that there would be enhancement from multiple particles, the Beer-Lambert law affects only the amplitude and not the location of the peak, nor does it scale by a non-linear factor, meaning that the ratio of the amplitudes of the scattering spectra at the various wavelengths is unchanged between the particle sizes with the application of Beer-Lambert. The net effect is that the scattering amplitudes can be reduced to arbitrary units, scaled to the scattering amplitude of the 80 nm particles at 532 nm, so chosen as the scattering cross-section of an 80 nm particle at 532 nm is 1×10^{-14} m^2. With the scattering profiles normalized, the same correlation graphs as previously shown for the absorbance can be created. The graphs are below in Figure 30.

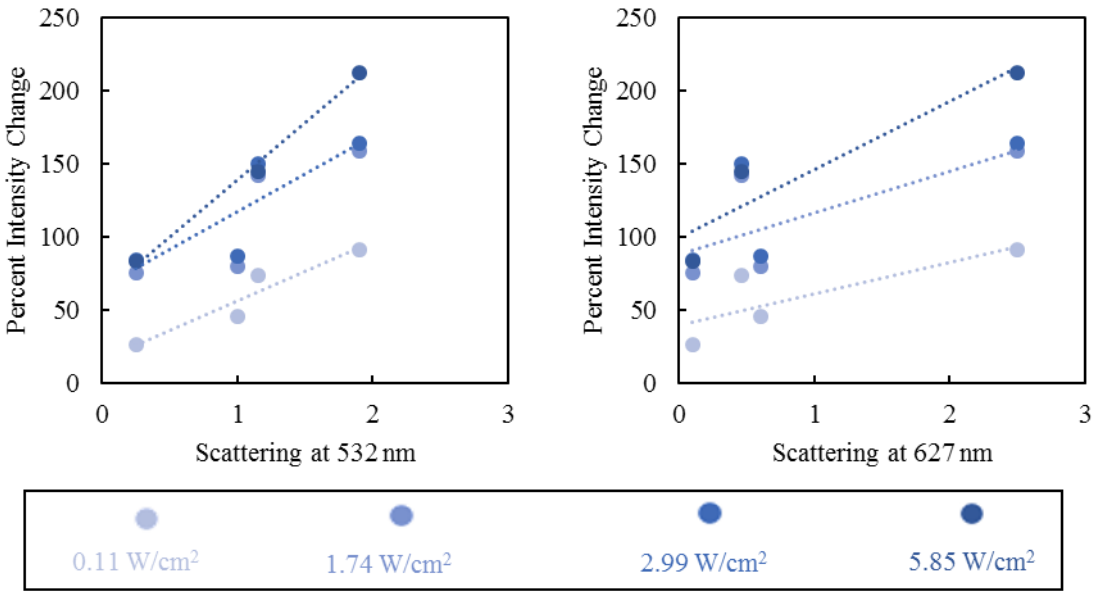

Figure 30 The correlation between scattering for (A) 532 nm and (B) 627 nm and photobrightening. The darker data points have a greater excitation intensity.

From Figure 30 it is clear that a weak correlation exists between the photobrightening change and the scattering at 627 nm. This indicates perhaps that the light emitted by the quantum dots hits the nanoparticles and scattered better toward the microscope objective than if there were

no nanoparticles. It is, however, a weak correlation. A much stronger correlation is present in the scattering at 532 nm. It is clear from the graph that there exists a strong correlation between the scattering at 532 nm and the photobrightening, leading to the conclusion that the scattered light is adding to the excitation of the quantum dots, and by virtue of the fact that quantum dots photobrighten more when exposed to a greater intensity of light, are photobrightening more as a result. The strong correlation between these variables makes this the most likely candidate. The consequences of this are two-fold. The first is support for the theory of optically-induced passivation of deep traps rather than increased thermal excitation, a claim reinforced by the low correlation between the absorbance at 532 nm and the photobrightening. If this were a thermal effect, it is to be expected that the greatest contribution would come from the absorbance of the excitation energy by the nanoparticles, thereby converting the electromagnetic energy to vibrational energy, inducing phonon contributions in the quantum dots. As this does not seem to be present, the phonon hypothesis can be discarded. To drive home this effect, Figure 28 and Figure 30 have been recreated below with the addition of lines of best fit. Those best fits make more clear the fact that there is a much stronger correlation for the scattering at 532 nm than any of the other three parameters. This is shown below in Figure 31.

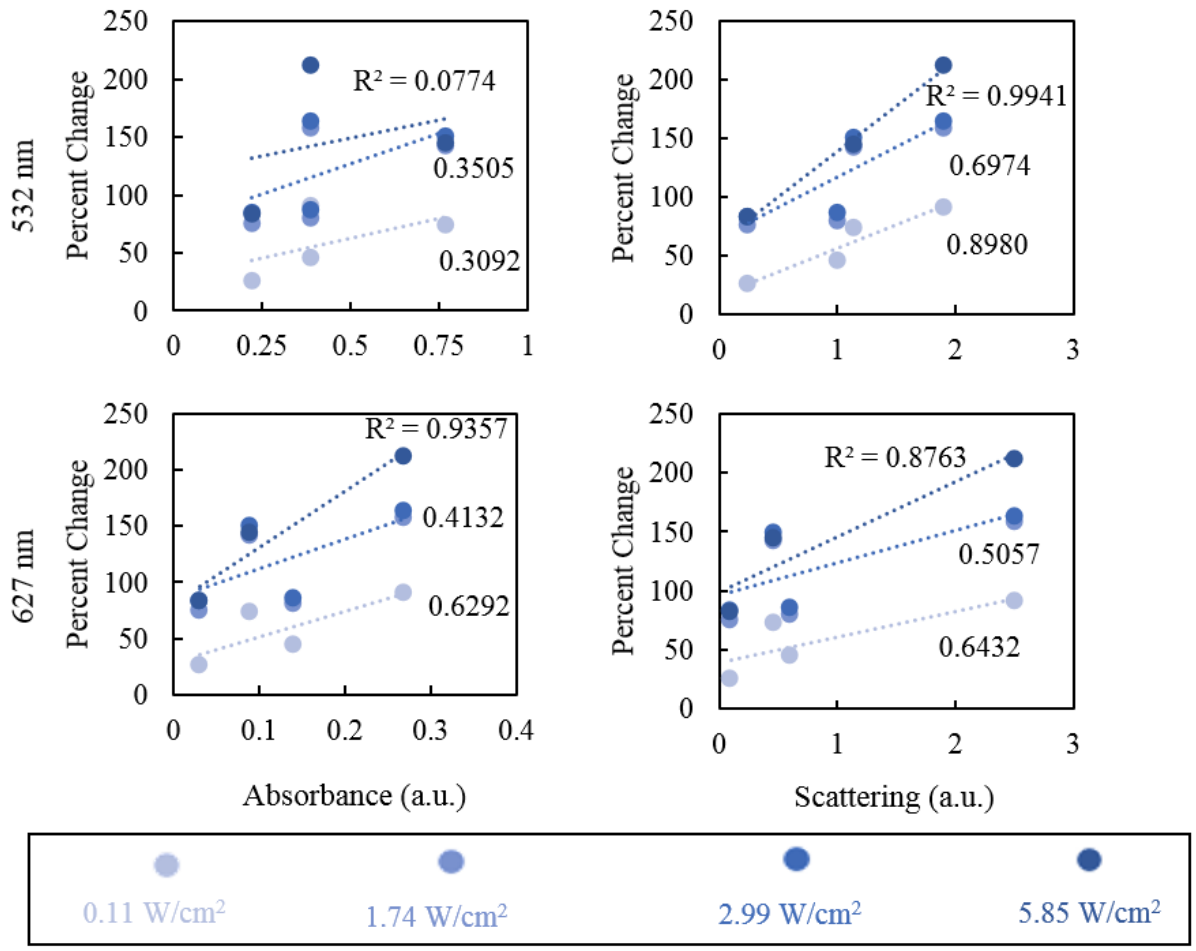

Figure 31 The correlations of the photobrightening with the several parameters of interest. (A) and (C) show the correlation with the absorbance at 532 nm and 627 nm, respectively, while (B) and (D) show the correlation with the scattering at 532 nm and 627 nm respectively. Like **Figure 28** and **Figure 30**, the darker data refers to more intense excitation energy. The dotted lines give the lines of best fit for each of the intensities.

Clear from Figure 31 is that there is a much closer fit for the scattering at 532 nm than any of the other parameters, shown by the coefficients of determination. For each excitation intensity, shown by the different colored lines, the coefficient of determination is greatest for the scattering at 532 nm. Similarly clear is that there is virtually no correlation between the photobrightening and the absorbance at 532, again discrediting the thermal effect hypothesis.

The second implication is that the enhancement of photobrightening can be achieved by nanostructures with large scattering cross-sections at the proper excitation wavelength. This leads to not only the obvious conclusion that nanoparticles can enhance photobrightening rather than damping it, but that quantum dots can be used to determine the optical enhancement of a given nanostructure at a certain wavelength, provided that the wavelength is below the emission wavelength of a quantum dot. There is the requirement that each set of fabricated quantum dots will need to be individually calibrated, but the photobrightening will be able to be used to verify the plasmonic enhancement.

ii. Nanospheres and Nanorods

Having exhausted the available nanospheres, the accompanying relative safety of the spherical geometry must now be fled for the more complex nature of other shapes. As the nanospheres were ordered from nanoComposix, additional geometric shapes were ordered from them as well, i.e. nanoshells and nanorods. The nanoshells are dual-layer spheres with a core of silicon and a gold shell. The two different sizes of nanoshells procured are defined by their absorbance peaks, one at 660 nm and the other at 800 nm. From the measurements made by nanoComposix, the 660 nm resonant nanoshells have a silica core with an 88 nm diameter and a gold shell of 35 nm, giving a total diameter of 159 nm. For the 800 nm nanoshells, there is a 120 nm diameter silica core and a gold shell thickness of 17 nm, giving an overall diameter of 153 nm. The nanorods are 48.4 nm in length and have a width of 17.4 nm, giving an aspect ratio of 2.8. Unfortunately, nanoComposix does not provide the scattering spectra for these particles. It is, nevertheless, important to make sure that the ideas presented here hold true. Even without the scattering spectra, it is enough to

verify that the presence of the nanoshells and nanorods will not cause quenching in the photobrightening.

Taking first the case of nanorods, as they are the same shape as the particles used in Chen's work. A note of difference is that the nanorods used here have a resonance peak at 660 nm, rather than the 800 nm used in Chen's paper. The rods in that paper caused the complete quenching of photobrightening, although not quenching the photoluminescence itself, as has been before reported[25], [66], [67], [69]. While it was not the case that the addition of nanospheres caused quenching, it is not unrealistic that the quenching could be based on the geometry shape, meaning that rods could behave differently than spheres. To that end, the same photobrightening experiment was conducted, using an excitation intensity of 1.74 W/cm^2. The same preparation procedures were followed as well. The result is illustrated below in Figure 32.

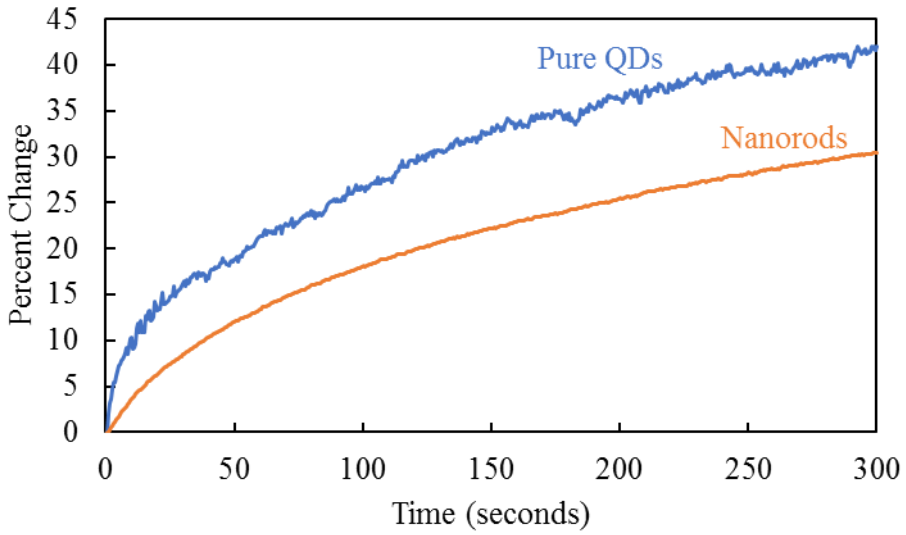

Figure 32 Photobrightening as a result of nanorods. The line for the nanorods is present in orange while the pure quantum dots are in blue.

From Figure 32 it seems that the nanorods do indeed cause photobrightening to be quenched, although not as drastically as in Chen's paper, seemingly a point in favor of the idea that nanoparticles cause quenching, or at least nanorods do. However, it is important to keep in mind the fact that quantum dots age over time, meaning that as these experiments with the nanorods were conducted months after the test of the pure quantum dots, the quantum dot response may have been diminished. Upon performing a new test of pure quantum dots, it becomes apparent that the quantum dots have diminished in their photobrightening, as shown in Figure 33.

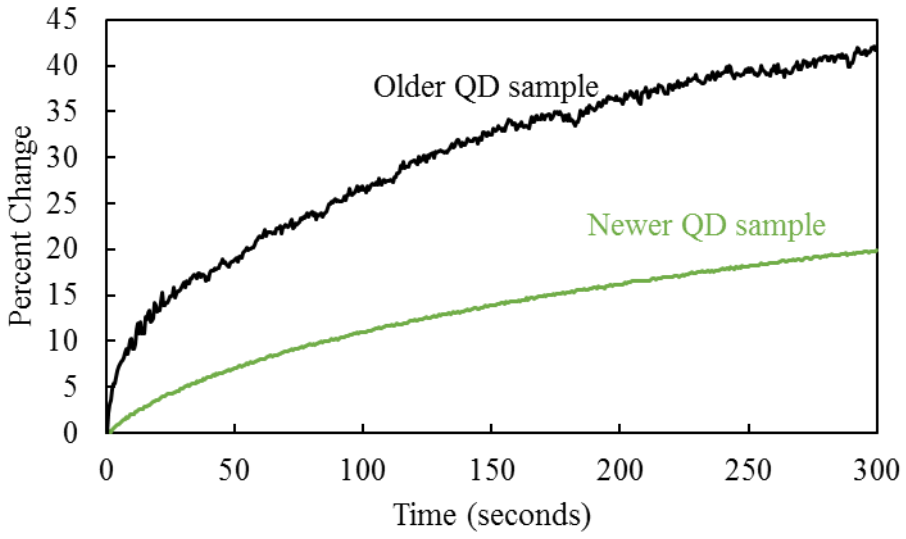

Figure 33 The effect of age on quantum dot photobrightening. The older quantum dots are shown in black and the newer sample is shown in green. These are from the same batch of quantum dots, simply deposited and tested months apart. These tests are conducted at an intensity of 1.74 W/cm^2.

Illustrated in Figure 33 is the difference which time can make in the photobrightening of the quantum dots. The quantum dots have still the ability to photobrighten, but it is clear that they are photobrightening by roughly half of the amount as previous, 19.9% vs. 42.1% Bearing in mind the difference in the photobrightening potential, the 30.5% by which the nanorods caused the nanorods to photobrighten can be viewed as about a 60% increase if they were tested

earlier in the life of the quantum dots. They would still not cause as high a photobrightening as the spheres, especially considering that the concentration of the nanorods is 1.14×10^{13} particles/mL, or about 2000 times as concentrated, but they do not, at least at this concentration, cause damping of the photobrightening.

The other geometry is that of the nanoshells. These should behave remarkable similarly to the nanospheres, based on the geometry, as each have a spherical cross-section for scattering. They do, however, have very different absorption peaks, one at 660 nm and one at 800 nm, as opposed to the nanospheres where the absorbance values range from about 530 nm to about 570 nm. The nanorods used in Chen's paper have a resonance peak at 800 nm, so assuming for the moment that it is the resonance peak which causes the damping of the photobrightening rather than the geometry, testing these particles should provide illumination, shown in Figure 34.

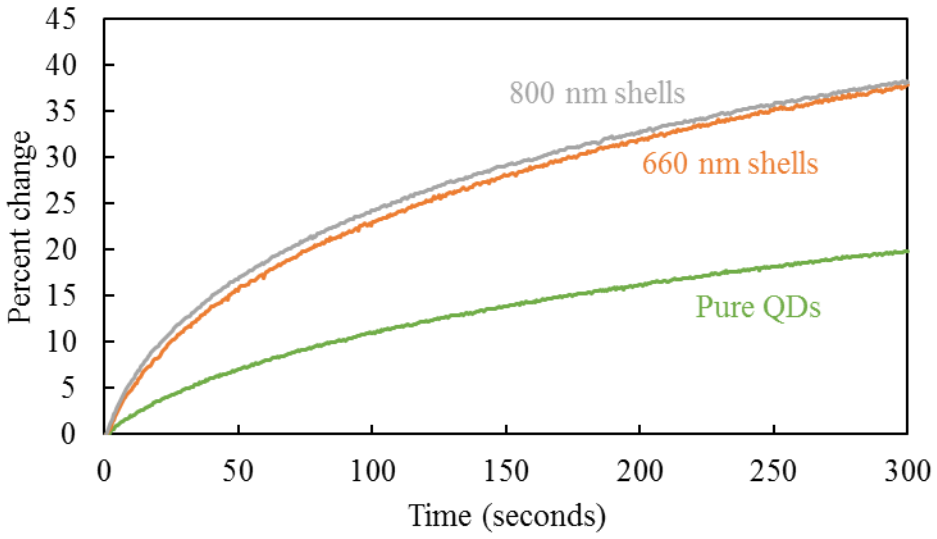

Figure 34 The photobrightening due to gold nanoshells. The listed wavelength for the shells (660 nm and 800 nm) are the resonance wavelength, not the sizes. In green are the quantum dots which were tested alongside the nanoshells.

As is apparent from Figure 34, the nanoshells cause just about equal photobrightening, both cause significantly more photobrightening than pure quantum dots. The photobrightening, compared to the newly tested quantum dots, reaches about 37% compared to about 20%, putting them in about the range of the 60 nm and 80 nm spheres after dilution. However, unlike the case of the nanorods presented earlier, these nanoshells are more dilute than the nanospheres, by a factor of 2-3 from the diluted spheres. This means that if they were of a similar concentration it is likely that they would cause significantly more photobrightening. The conclusion to be drawn from this is that even though the resonance of the nanoshells is the same as the nanorods presented in Chen's work (800 nm), there is still photobrightening above and beyond the case without plasmonic nanoparticles. With this final test, the idea that plasmonic nanoparticles will assuredly cause quenching in photobrightening can finally be put to rest.

CHAPTER VI. METASURFACES

i. Background

Having now discussed the several particles available and finding photobrightening to be enhanced by all of them, attention can now be paid to designed structures. The previous studies were conducted with randomly distributed particles deposited on top of quantum dots. This is not, however, reflective of many likely conditions for real world devices. More likely is the design whereby the metal structure is first designed and then quantum dots are deposited on top. While there are structures that have been made and are readily available for use as test beds for quantum dots, they have a distinct problem of being difficult to align to the system and having few chances to test. The reason for the difficult alignment is that the quantum dots, as have now be repeatedly shown, have a time dependence which is what is being tested. The light for alignment would also begin activation if the experiment is not properly designed and administered. The best way around this problem is to use a different wavelength of light for alignment, one which is longer than the emission wavelength of the quantum dots and hence does not begin the photobrightening process. Barring such a light being readily available, as was the case here, a different solution is needed. As the trouble was alignment, an easy solution is to increase the size of the device, thereby removing, at least to some extent, the alignment problem.

Enter metasurfaces. Metasurfaces are arrays of ordered nanostructures which cause interesting effects when illuminated by light which is of a larger wavelength than the structures of the array[70]–[73]. These have incredible potential for numerous applications including antennae[74], [75], sensors[76], [77], displays[78], [79], and even cloaking[80], [81]. Creating these structures surfaces can be done in ways as varied as their uses[82]. One method in particular uses a chemical reaction to cause nanoparticles to arrange themselves in an ordered fashion on a surface[83], creating a hexagonally packed array of nanospheres. The spheres used there have a

diameter of 13 nm. Some of the same samples used in that paper were obtained for use with quantum dots to study the plasmonic effect of the metasurfaces on the photobrightening process. Similar to the earlier chapters, the materials used are gold nanospheres, although admittedly smaller than those used before. The nanospheres are here 13 nm in diameter, making them roughly the size of the quantum dots. However, the self-assembled nanoparticle surface must, by its very nature, be placed on the substrate first. This is a stark departure from the previous work with nanoparticles as they had always been placed over the quantum dots. They are also deposited on glass and not silicon. This difference means that the photoluminescence experiment will have some issues.

The metasurfaces are created using a chemical reaction which promotes the growth of a self-assembled layer of nanospheres on a surface. This layer grows out of a liquid up the side of the surface being used. Each surface is made using 13 nm spheres, but there is a protective shell of ligands surrounding each sphere. These ligands create spacers, preventing the gold spheres from coming into contact, leaving nanoscale gaps between the spheres. It is these gaps which provide the interesting phenomena giving credence to the label of metasurfaces. The gap size is controlled through the ligand size, allowing for easy tunability in the size of the gaps. The ligands are created from alkanethiols and associated alkane dithiols, with the size of the ligands determined by the number of carbon atoms in the molecule. The gap size as a function of the thiol length is shown in Figure 35, here reused with permission from [83].

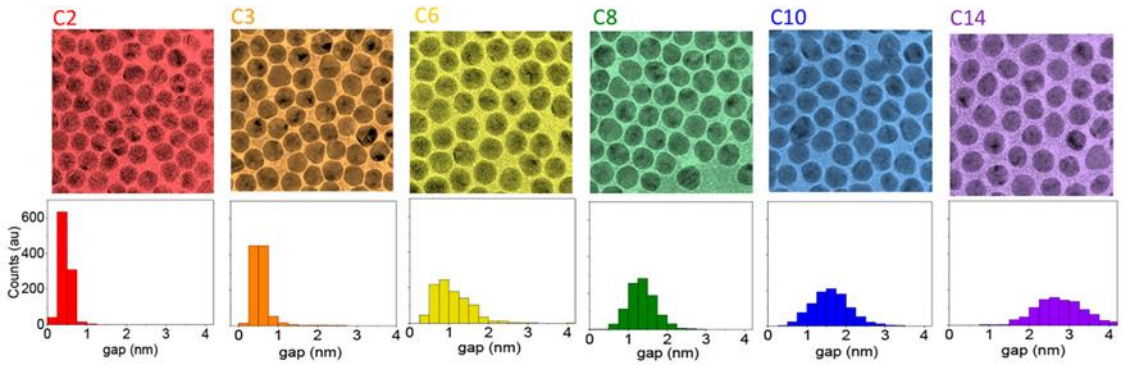

Figure 35 TEM images (top) and interparticle gaps distributions (bottom) for various ligand sizes. The images have had a false color applied to them to more easily differentiate the gap sizes. The listed C-number gives the number of carbon atoms in the ligand. Reprinted with permission from D. Doyle et al., "Tunable Subnanometer Gap Plasmonic Metasurfaces," ACS Photonics, vol. 5, no. 3, pp. 1012–1018. Copyright 2018 American Chemical Society

From Figure 35, it is clear that the ligand size has a great effect on the gap size. There are also certain portions which appear to have holes in the lattice where nanospheres should be. Minor imperfections such as these do occur and cause a change in the effects at that point in the lattice. This is, it should be said, a relatively minor issue as the region affected is on the order of nanometers and the observed regions for the photobrightening are on the order of around 100 nm, making the missing spheres likely a minor inconvenience rather than a point of concern. It is also clear that the larger gaps result in more varied gap size ranges. Putting into a table the data from the images gives the following:

Table 2 Metasurface gap size based on ligand length

Ligand	Gap size (nm)	Error (nm)
C-2	0.45	±0.14
C-3	0.55	±0.22
C-6	1.1	±0.46
C-8	1.4	±0.37
C-10	1.6	±0.48
C-14	2.8	±0.69

The gap sizes shown in the table lay obvious the fact that the gaps are significantly smaller than the quantum dots. Because of this, the quantum dots will be resting on top of the surface rather than being in one of the gap regions with the higher electric field, meaning that they are unlikely to photobrighten as much as when combined with the nanoparticles from earlier. The differing gaps cause different behaviors in the interaction of the incident light with the local surface plasmons induced. While it is not easily possible to obtain scattering data, the absorption data is readily available. The data was collected using random regions of the several samples and is shown in Figure 36.

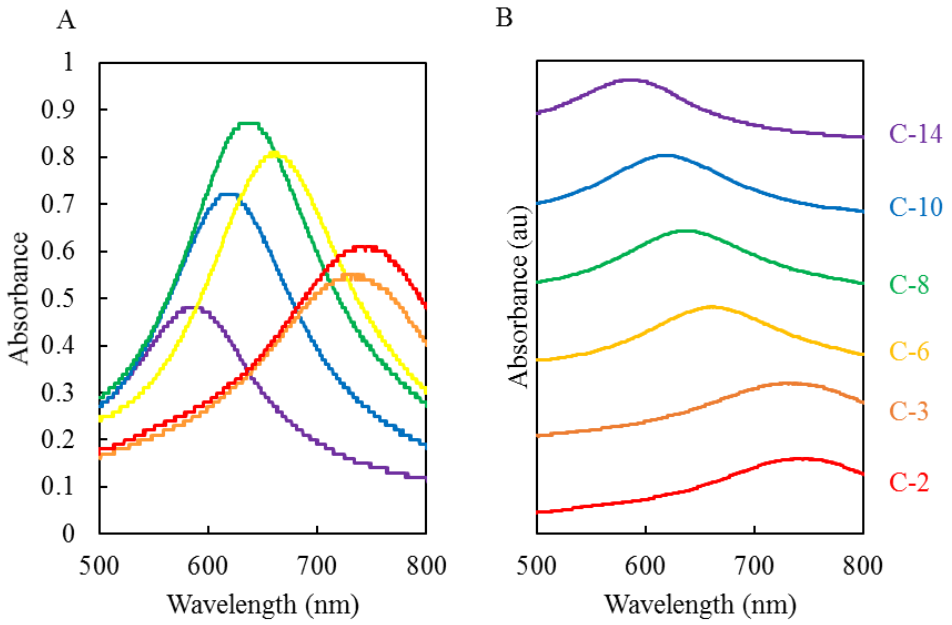

Figure 36 (A) The absorbance spectra for the metasurfaces of various ligand lengths. (B) The same absorbance spectra as (A) normalized to the maximum value of each spectrum and arranged as a waterfall in order of ligand length, shortest being at the bottom.

Figure 36 illustrates the effect which the gap size can have on the absorption spectrum. As the gap gets larger, the peak shifts toward the blue; an explanation for this phenomenon can be found in [83]. Ideally, this would mean that the metasurfaces with the longest ligands should have the greatest enhancement of the 532 nm excitation light. However, based on the results of Figure 36 (A), this is not necessarily the case.

ii. Experimental Results

The samples selected for characterization were C-2, C-8, and C-14, chosen for the wide range of ligand sizes represented. To prepare the samples for characterization, a modified preparation method was used. To apply acetone and isopropyl alcohol for cleaning would be to

damage or remove the metasurfaces, so those steps were omitted. This does cause the issue of the samples not being clean, which may account for the difference in the absorbance values from the prediction as shown in Figure 36. The quantum dots were sonicated for one minute in a hot water bath to create an even dispersion of the quantum dots within the suspension. A single drop of quantum dot solution was deposited on each metasurfaces and allowed to dry for 48 hours. Because the metasurfaces are grown on glass and not on silicon, a drop of the quantum dots was also deposited on a section of one of the glass substrates without the metasurface. This was used as the baseline.

Each sample was loaded in turn into the same photoluminescence setup as before. There is, though, a difficulty which arises when bringing the sample into focus caused by the transparent nature of the substrate. When focusing the sample, the sample stage is first moved to the position farthest from the microscope objective. While watching the image on the camera the stage is moved forward until it is in focus. The reason for this elaborate procedure is that there are two focal points for the laser, one on the front face of the sample and one on the back face. Were the sample to be moved forward to this secondary focus, the quantum dots would not be in focus as they have been deposited only on the front of the sample. Having now solved this truly trivial problem, the photobrightening experiments can now be performed, the results of which are shown in Figure 37.

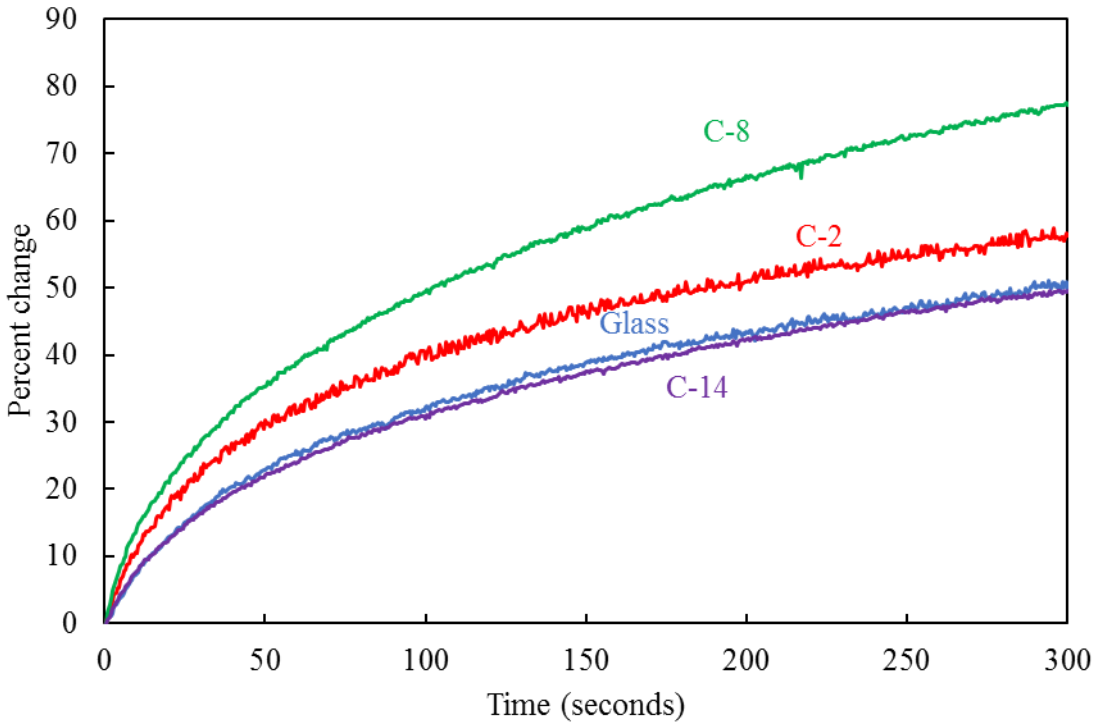

Figure 37 Photobrightening effects of plasmonic metasurfaces. The blue line represents quantum dots on glass alone; the other surfaces tested were C-2 (red), C-8 (green), and C-14 (purple), representing ligand lengths of .45 nm, 1.4 nm, and 2.8 nm, respectively.

The photobrightening tests reveal an interesting and unexpected result. The glass still allows photobrightening of the quantum dots, as expected based on previous experiments. The photobrightening has been decreased from the case of the silicon substrate, although whether that is the elapsed time or the transparent nature of the glass is not determined. The smallest gap also produced limited brightening, also as expected. Additionally, there is a significant photobrightening enhancement by the C-8 metasurface with a gap size of 1.4 nm. Based on the absorbance data, which is of otherwise limited use as scattering, not absorbance, is the dominant factor, the largest brightening coming from the C-8 metasurface is not entirely unexpected as the largest absorbance value is there present. What is surprising is the result from C-14. This is a

metasurface with a ligand length of 2.8 nm, giving it an absorbance peak around 586 nm. The fact that it has such a low absorbance peak wavelength means that it would seem the most likely to enhance the excitation light at 532 nm. Looking at the absorbance at 532 nm, the metasurface does not have the highest absorbance value, but it is still significantly higher than the absorbance value of the C-2 metasurface. This is shown in Figure 38.

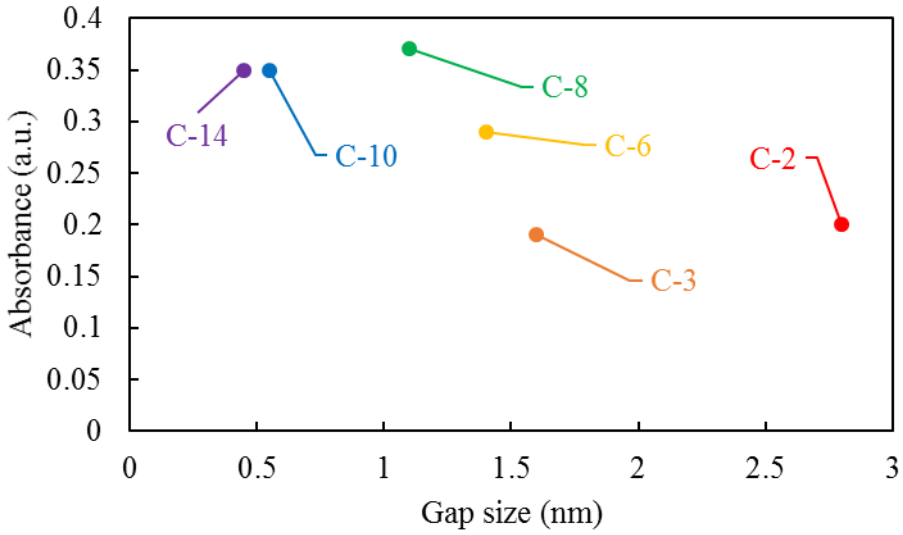

Figure 38 The absorbance at 532 nm of the various metasurfaces.

Figure 38 illustrates the problem clearly, although also serves to again drive home the point that the absorbance at the excitation wavelength does not correlate with the photobrightening. With the available instrumentation it was not possible to determine the scattering spectra for the metasurfaces due to the fact that the samples are on a glass substrate. However, as pointed out earlier, one of the main factors in determining the photobrightening is the optical enhancement. Using COMSOL, a simulation was developed to calculate the optical enhancement of the metasurfaces. This uses a set of mirrored boundary conditions to simulate an essentially infinite grid of gold nanoparticles. The distance between the nanoparticles is simulated for each of the three gap widths tested experimentally. Below the nanoparticles is glass and the remainder of the

simulation space is filled with air. Like the previous simulations, a light wave is simulated originating at the top of the simulation and traveling downward with the electric field polarized in the x-direction. While there are simulations which illustrate the large enhancement in the gap between the nanoparticles, this gap is too small for the quantum dots to fit. A slice of the optical enhancement field ($|E/E_0|^2$) was therefore taken at a distance of 2 nm above the top of the nanospheres. For this reason, the slice does not display a large enhancement in what would appear to be the gap region. These slices were taken for each of the three gap sizes and the results are displayed below in the next several figures. Each of the slices uses the same color scale to display the optical enhancement although the maximum and minimum values will be different.

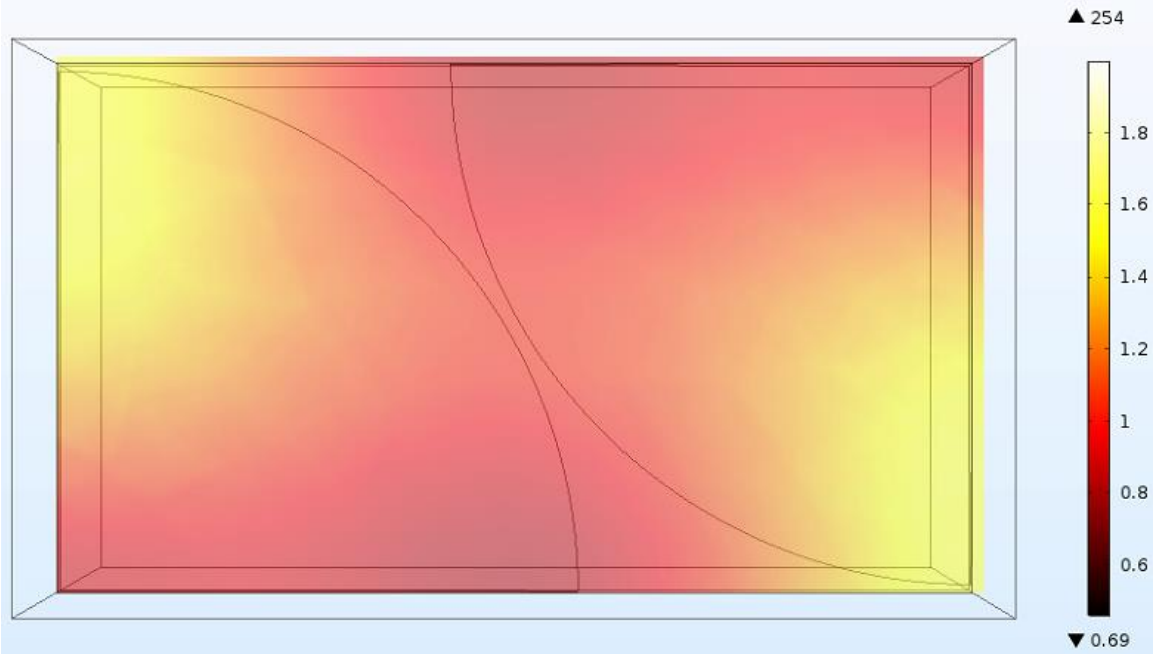

Figure 39 The optical enhancement for the C-2 metasurface with a minimum gap size of 0.45 nm. The black lines show the outline of the surfaces simulated. The regions with the greatest enhancement are in the upper-left and lower-right corners.

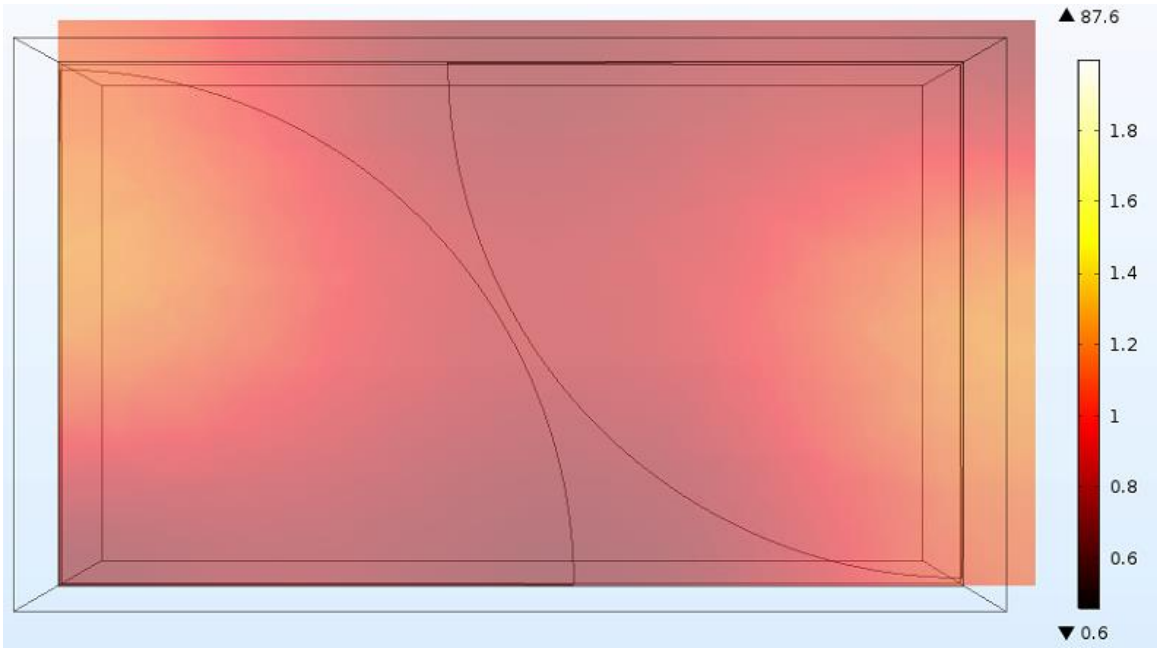

Figure 40 The optical enhancement for the C-8 metasurface with a minimum gap size of 1.4 nm. The region of greatest enhancement has moved from the previous figure toward the centers of the spheres. The slice extends outside of the black outline of the frame due to simulation methodology

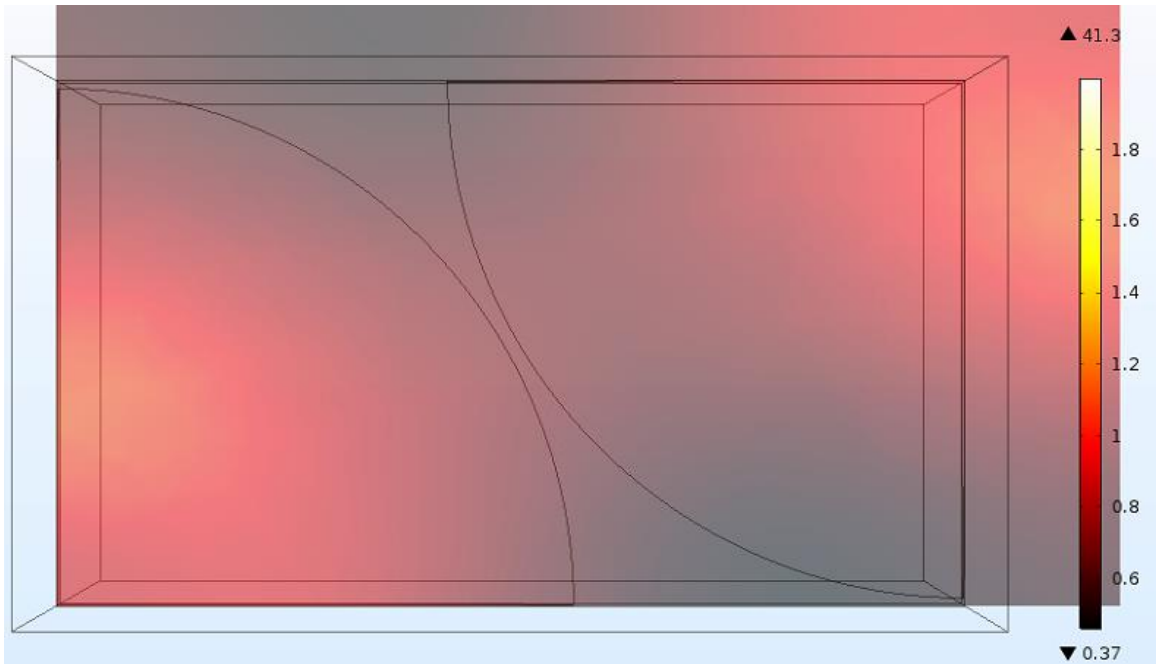

Figure 41 The optical enhancement for the C-14 metasurface with a minimum gap size of 2.8 nm. The regions of greatest enhancement have moved farther toward the center of the spheres.

From the figures, it is clear that the greatest enhancement values are present in the simulation with the smallest minimum gap size, as expected from many plasmonic works studying the effect of gap size on optical enhancement [6], [13], [16], [21], [37], [83]. Looking at Figure 41, the fact that the C-14 metasurface does not seem to cause a greater photobrightening than the glass substrate can now be readily explained by the fact that a large portion of the slice of the optical enhancement features optical enhancement values below 1, indicating a damping effect. While this is not intended to give exact values for use later, it does provide, as with so much of this work, evidence of an effect and a plausible cause for said effect.

CHAPTER VII. CONCLUSION AND FUTURE WORK

i. Conclusion

The rapid development of quantum dot technology requires a deeper understanding of the behavior exhibited. The most important aspect of quantum dots for applications is the wavelength and amplitude of the emitted light. The wavelength is highly tunable, and easily so based on the preparation time and the materials used. Amplitude can be affected by numerous factors, among which is the excitation energy, the two most common sources of energy are electrical currents and electromagnetic waves (light). For a given intensity of excitation light there are ways of enhancing the intensity of the emitted light from the quantum dots. The most common of these are the addition of plasmonic nanoparticles or the use of continuous light rather than the pulsed light used most often. The continued excitation of the quantum dots via light causes increased photoluminescence over time, known as photobrightening. While it is not a new idea that photobrightening, or, as it has also been called, photoenhancement, takes place the study of physical parameters which enhance the photobrightening is a subject which has in the past received little attention.

The intensity of quantum dots has been shown to increase logarithmically with the intensity of the emitted light both here and in previous work. The increase of the initial intensity by plasmonic enhancement is not the same as the increase over time with continued laser exposure, a process which is still not well understood. This increase over time also has several factors which affect it, one of which is the intensity of the excitation light. Based on the work here presented, this photobrightening is altered by increased excitation light in a linear fashion. By subjecting quantum dots deposited on a silicon substrate to multiple different intensities of excitation light and studying the response it has been made clear that not only does the excitation light have a

noticeable and measurable effect on the photobrightening, but that effect is linear with the excitation intensity. The linear increase makes possible to ascertain the intensity of the light received by the quantum dots, thereby allowing for the determination of the electric field which is stimulating the emission and photobrightening behavior of the quantum dots.

While previous studies have stated that the addition of metallic nanoparticles will cause the quantum dot photobrightening to be quenched, as has also been shown to be the case with quantum dots placed near large electron acceptors such as bulk metals, the findings presented here demonstrate that not only is the photobrightening not necessarily quenched, it can, in fact, be increased. The presence of the nanoparticles allows for the increase of the excitation light via plasmonic optical enhancement, and not, as my have been hypothesized, phonon effects. As the plasmonic nanoparticles have been found to increase the initial intensity of the quantum dots, it is not unexpected that they would also increase the photobrightening. The increased photobrightening via plasmonic enhancement means that the quantum dots can be made brighter as desired by tuning the plasmonic resonance wavelength to the desired excitation wavelength and that the photobrightening of quantum dots in the presence of a given nanostructure can give an experimental method of determining the plasmonic enhancement of a given wavelength from a fabricated nanostructure. There is, of course a continued need for more studies, but this dissertation gives proof-of-concept and a foundation for future works.

ii. Future Work

The quantum dots presented here are not dissimilar to the quantum dots used in numerous applications including sensors, displays, and solar cells, along with a host of other applications.

The use of quantum dots as either displays or detectors means that the intensity of the light emitted by the quantum dots is of utmost importance. Despite reports that the intensity of the quantum dots is unchanged over time as found in other works, the results gathered from the experimental results in this work show that the intensity of the quantum dots can increase over time, especially on the short-term scale. Additionally, many of these applications have the potential to utilize plasmonic particles to enhance the effects of the quantum dots, so an understanding of how these nanoparticles are interacting with the quantum dots on a case-by-case basis is vital. The effects of these can be modeled by finite element method computational software but, as presented here, the computational models cannot accurately simulate all of the real-world complexities involved. To proceed, the structures which are commonly used in real-world applications should be fabricated and tested with the quantum dots present in order to determine what, if any, effects the designs of the structures have on the time-dependent behavior of the quantum dots.

An experimental determination of the plasmonic enhancement is perhaps the most important extension of this work. In order to do that, there are several steps that must be undertaken in future work. All quantum dots which will be used for testing must be characterized first without depositing them on the nanostructure in question. The substrate used for the devices makes a large difference in the photobrightening and must be taken into account. The quantum dots will also have differing behaviors based on the position of the quantum dots within the device and so a method of placing these within the devices at specified locations without photoactivation, electro-activation, or any other sort of effects which can cause time-dependent responses. This is a problem which must be solved before the phenomenon presented here can be used for experimental verification of computational simulations. As many plasmonic nanodevices created

will have features below 10 nm, there is, perhaps, a limited amount of sensitivity which these quantum dots can provide, but it is not insignificant. Similarly, smaller quantum dots could fit into smaller gap sizes while still keeping the ability to photobrighten, providing increasingly fine probing abilities. There are, of course, computational models which can provide insight to the effects expected. The experimental verification of those models would be a boon to future research; similarly, the results of the experiments can be used to bolster the simulations and be used to fix problems present.

Having now exhausted the photobrightening effects due to plasmonic behavior, this work can also be expanded to include other factors not here taken into account, such as temperature dependence, the humidity of the environment, and the atmospheric quality. Each of these factors has the potential to affect the intensity of the quantum dots, and, more importantly, affect the evolution of this intensity over time. With a basis formed by the work here presented, these factors can be individually examined, and the time-dependent behaviors glossed over in other papers can be accounted for, allowing for new information to be gained from old works.

CHAPTER VIII. BIBLIOGRAPHY

[1] S. Law, V. Podolskiy, and D. Wasserman, "Towards nano-scale photonics with micro-scale photons: the opportunities and challenges of mid-infrared plasmonics," *Nanophotonics*, vol. 2, no. 2, Jan. 2013.

[2] S. A. Maier and H. A. Atwater, "Plasmonics: Localization and guiding of electromagnetic energy in metal/dielectric structures," *J. Appl. Phys.*, vol. 98, no. 1, p. 011101, Jul. 2005.

[3] S. A. Maier, M. L. Brongersma, P. G. Kik, S. Meltzer, A. a. G. Requicha, and H. A. Atwater, "Plasmonics—A Route to Nanoscale Optical Devices," *Adv. Mater.*, vol. 13, no. 19, pp. 1501–1505, Oct. 2001.

[4] H. A. Atwater and A. Polman, "Plasmonics for improved photovoltaic devices," *Nat. Mater.*, vol. 9, no. 3, pp. 205–213, Mar. 2010.

[5] P. K. Ghosh, D. T. Debu, D. A. French, and J. B. Herzog, "Calculated thickness dependent plasmonic properties of gold nanobars in the visible to near-infrared light regime," *PLOS ONE*, vol. 12, no. 5, p. e0177463, May 2017.

[6] S. J. Bauman, E. C. Novak, D. T. Debu, D. Natelson, and J. B. Herzog, "Fabrication of Sub-Lithography-Limited Structures via Nanomasking Technique for Plasmonic Enhancement Applications," *IEEE Trans. Nanotechnol.*, vol. 14, no. 5, pp. 790–793, Sep. 2015.

[7] K. R. Catchpole and A. Polman, "Plasmonic solar cells," *Opt. Express*, vol. 16, no. 26, pp. 21793–21800, Dec. 2008.

[8] V. E. Ferry *et al.*, "Light trapping in ultrathin plasmonic solar cells," *Opt. Express*, vol. 18, no. 102, pp. A237–A245, Jun. 2010.

[9] K. Nakayama, K. Tanabe, and H. A. Atwater, "Plasmonic nanoparticle enhanced light absorption in GaAs solar cells," *Appl. Phys. Lett.*, vol. 93, no. 12, p. 121904, Sep. 2008.

[10] S. Bauman *et al.*, "Substrate Oxide Layer Thickness Optimization for a Dual-Width Plasmonic Grating for Surface-Enhanced Raman Spectroscopy (SERS) Biosensor Applications," *Sensors*, vol. 17, no. 7, p. 1530, Jun. 2017.

[11] A. Hassani and M. Skorobogatiy, "Photonic crystal fiber-based plasmonic sensors for the detection of biolayer thickness," *J. Opt. Soc. Am. B*, vol. 26, no. 8, p. 1550, Aug. 2009.

[12] M. Potara, A.-M. Gabudean, and S. Astilean, “Solution-phase, dual LSPR-SERS plasmonic sensors of high sensitivity and stability based on chitosan-coated anisotropic silver nanoparticles,” *J. Mater. Chem.*, vol. 21, no. 11, p. 3625, 2011.

[13] T. Siegfried, Y. Ekinci, H. H. Solak, O. J. F. Martin, and H. Sigg, “Fabrication of sub-10 nm gap arrays over large areas for plasmonic sensors,” *Appl. Phys. Lett.*, vol. 99, no. 26, p. 263302, Dec. 2011.

[14] L. Tong *et al.*, “Recent Advances in Plasmonic Sensors,” *Sensors*, vol. 14, no. 5, pp. 7959–7973, May 2014.

[15] A. A. Darweesh, S. J. Bauman, D. A. French, A. Nusir, O. Manasreh, and J. B. Herzog, “Current Density Contribution to Plasmonic Enhancement Effects in Metal-Semiconductor-Metal Photodetectors,” *J. Light. Technol.*, vol. 36, no. 12, pp. 2430–2434, Jun. 2018.

[16] J. Theiss, P. Pavaskar, P. M. Echternach, R. E. Muller, and S. B. Cronin, “Plasmonic Nanoparticle Arrays with Nanometer Separation for High-Performance SERS Substrates,” *Nano Lett.*, vol. 10, no. 8, pp. 2749–2754, Aug. 2010.

[17] J. Ye *et al.*, “Plasmonic Nanoclusters: Near Field Properties of the Fano Resonance Interrogated with SERS,” *Nano Lett.*, vol. 12, no. 3, pp. 1660–1667, Mar. 2012.

[18] H. T. Ngo, H.-N. Wang, A. M. Fales, and T. Vo-Dinh, “Plasmonic SERS biosensing nanochips for DNA detection,” *Anal. Bioanal. Chem.*, vol. 408, no. 7, pp. 1773–1781, Mar. 2016.

[19] D. T. Debu, P. K. Ghosh, D. French, and J. B. Herzog, “Surface plasmon damping effects due to Ti adhesion layer in individual gold nanodisks,” *Opt. Mater. Express*, vol. 7, no. 1, p. 73, Jan. 2017.

[20] D. T. Debu, S. J. Bauman, D. French, H. O. H. Churchill, and J. B. Herzog, “Tuning Infrared Plasmon Resonance of Black Phosphorene Nanoribbon with a Dielectric Interface,” *Sci. Rep.*, vol. 8, no. 1, Dec. 2018.

[21] A. A. Darweesh, S. J. Bauman, and J. B. Herzog, “Improved optical enhancement using double-width plasmonic gratings with nanogaps,” *Photonics Res.*, vol. 4, no. 5, pp. 173–180, Oct. 2016.

[22] A. Vial, “Implementation of the critical points model in the recursive convolution method for modelling dispersive media with the finite-difference time domain method,” *J. Opt. Pure Appl. Opt.*, vol. 9, no. 7, p. 745, 2007.

[23] Y. Zhao and Y. Hao, "Finite-Difference Time-Domain Study of Guided Modes in Nano-Plasmonic Waveguides," *IEEE Trans. Antennas Propag.*, vol. 55, no. 11, pp. 3070–3077, Nov. 2007.

[24] K. Tanaka, E. Plum, J. Y. Ou, T. Uchino, and N. I. Zheludev, "Multifold Enhancement of Quantum Dot Luminescence in Plasmonic Metamaterials," *Phys. Rev. Lett.*, vol. 105, no. 22, Nov. 2010.

[25] V. V. Breus, C. D. Heyes, and G. U. Nienhaus, "Quenching of CdSe−ZnS Core−Shell Quantum Dot Luminescence by Water-Soluble Thiolated Ligands," *J. Phys. Chem. C*, vol. 111, no. 50, pp. 18589–18594, Dec. 2007.

[26] J. M. Costa-Fernández, R. Pereiro, and A. Sanz-Medel, "The use of luminescent quantum dots for optical sensing," *TrAC Trends Anal. Chem.*, vol. 25, no. 3, pp. 207–218, Mar. 2006.

[27] X. Gao, Y. Cui, R. M. Levenson, L. W. K. Chung, and S. Nie, "*In vivo* cancer targeting and imaging with semiconductor quantum dots," *Nat. Biotechnol.*, vol. 22, no. 8, pp. 969–976, Aug. 2004.

[28] D. I. Son *et al.*, "Emissive ZnO–graphene quantum dots for white-light-emitting diodes," *Nat. Nanotechnol.*, vol. 7, no. 7, pp. 465–471, Jul. 2012.

[29] N.-M. Park, T.-S. Kim, and S.-J. Park, "Band gap engineering of amorphous silicon quantum dots for light-emitting diodes," *Appl. Phys. Lett.*, vol. 78, no. 17, pp. 2575–2577, Apr. 2001.

[30] S. Kim, B. Fisher, H.-J. Eisler, and M. Bawendi, "Type-II Quantum Dots: CdTe/CdSe(Core/Shell) and CdSe/ZnTe(Core/Shell) Heterostructures," *J. Am. Chem. Soc.*, vol. 125, no. 38, pp. 11466–11467, Sep. 2003.

[31] V. Aroutiounian, S. Petrosyan, A. Khachatryan, and K. Touryan, "Quantum dot solar cells," *J. Appl. Phys.*, vol. 89, no. 4, pp. 2268–2271, Jan. 2001.

[32] A. J. Nozik, "Quantum dot solar cells," *Phys. E Low-Dimens. Syst. Nanostructures*, vol. 14, no. 1, pp. 115–120, Apr. 2002.

[33] R. P. Raffaelle, S. L. Castro, A. F. Hepp, and S. G. Bailey, "Quantum dot solar cells," *Prog. Photovolt. Res. Appl.*, vol. 10, no. 6, pp. 433–439, Sep. 2002.

[34] A. Polimeni, A. Patanè, M. Henini, L. Eaves, and P. C. Main, "Temperature dependence of the optical properties of I n A s / A l y Ga 1 − y As self-organized quantum dots," *Phys. Rev. B*, vol. 59, no. 7, pp. 5064–5068, Feb. 1999.

[35] D. Valerini, A. Cretí, M. Lomascolo, L. Manna, R. Cingolani, and M. Anni, "Temperature dependence of the photoluminescence properties of colloidal Cd Se ⁄ Zn S core/shell quantum dots embedded in a polystyrene matrix," *Phys. Rev. B*, vol. 71, no. 23, Jun. 2005.

[36] C. de Mello Donegá, M. Bode, and A. Meijerink, "Size- and temperature-dependence of exciton lifetimes in CdSe quantum dots," *Phys. Rev. B*, vol. 74, no. 8, Aug. 2006.

[37] T. B. Hoang, G. M. Akselrod, C. Argyropoulos, J. Huang, D. R. Smith, and M. H. Mikkelsen, "Ultrafast spontaneous emission source using plasmonic nanoantennas," *Nat. Commun.*, vol. 6, no. 1, Dec. 2015.

[38] D. Pacifici, H. J. Lezec, and H. A. Atwater, "All-optical modulation by plasmonic excitation of CdSe quantum dots," *Nat. Photonics*, vol. 1, no. 7, pp. 402–406, Jul. 2007.

[39] Y.-H. Chan, J. Chen, Q. Liu, S. E. Wark, D. H. Son, and J. D. Batteas, "Ultrasensitive Copper(II) Detection Using Plasmon-Enhanced and Photo-Brightened Luminescence of CdSe Quantum Dots," *Anal. Chem.*, vol. 82, no. 9, pp. 3671–3678, May 2010.

[40] B. Omogo, F. Gao, P. Bajwa, M. Kaneko, and C. D. Heyes, "Reducing Blinking in Small Core–Multishell Quantum Dots by Carefully Balancing Confinement Potential and Induced Lattice Strain: The 'Goldilocks' Effect," *ACS Nano*, vol. 10, no. 4, pp. 4072–4082, Apr. 2016.

[41] C. D. Heyes, A. Y. Kobitski, V. V. Breus, and G. U. Nienhaus, "Effect of the shell on the blinking statistics of core-shell quantum dots: A single-particle fluorescence study," *Phys. Rev. B*, vol. 75, no. 12, Mar. 2007.

[42] J. Park and S.-W. Kim, "CuInS2/ZnS core/shell quantum dots by cation exchange and their blue-shifted photoluminescence," *J. Mater. Chem.*, vol. 21, no. 11, p. 3745, 2011.

[43] Y. Zhang *et al.*, "Time-Dependent Photoluminescence Blue Shift of the Quantum Dots in Living Cells: Effect of Oxidation by Singlet Oxygen," *J. Am. Chem. Soc.*, vol. 128, no. 41, pp. 13396–13401, Oct. 2006.

[44] W. G. J. H. M. van Sark, P. L. T. M. Frederix, A. A. Bol, H. C. Gerritsen, and A. Meijerink, "Blueing, Bleaching, and Blinking of Single CdSe/ZnS Quantum Dots," *ChemPhysChem*, vol. 3, no. 10, pp. 871–879, Oct. 2002.

[45] I. Robel, M. Kuno, and P. V. Kamat, "Size-Dependent Electron Injection from Excited CdSe Quantum Dots into TiO_2 Nanoparticles," *J. Am. Chem. Soc.*, vol. 129, no. 14, pp. 4136–4137, Apr. 2007.

[46] S. R. Cordero, P. J. Carson, R. A. Estabrook, G. F. Strouse, and S. K. Buratto, “Photo-Activated Luminescence of CdSe Quantum Dot Monolayers,” *J. Phys. Chem. B*, vol. 104, no. 51, pp. 12137–12142, Dec. 2000.

[47] M. Jones, J. Nedeljkovic, R. J. Ellingson, A. J. Nozik, and G. Rumbles, “Photoenhancement of Luminescence in Colloidal CdSe Quantum Dot Solutions,” *J. Phys. Chem. B*, vol. 107, no. 41, pp. 11346–11352, Oct. 2003.

[48] O. Kulakovich *et al.*, “Enhanced Luminescence of CdSe Quantum Dots on Gold Colloids,” *Nano Lett.*, vol. 2, no. 12, pp. 1449–1452, Dec. 2002.

[49] K. Okamoto, S. Vyawahare, and A. Scherer, “Surface-plasmon enhanced bright emission from CdSe quantum-dot nanocrystals,” *J. Opt. Soc. Am. B*, vol. 23, no. 8, p. 1674, Aug. 2006.

[50] D. R. Cooper *et al.*, “Photoenhancement of lifetimes in CdSe/ZnS and CdTe quantum dot-dopamine conjugates,” *Phys. Chem. Chem. Phys.*, vol. 11, no. 21, pp. 4298–4310, May 2009.

[51] J. A. Kloepfer, S. E. Bradforth, and J. L. Nadeau, “Photophysical Properties of Biologically Compatible CdSe Quantum Dot Structures,” *J. Phys. Chem. B*, vol. 109, no. 20, pp. 9996–10003, May 2005.

[52] J. Hill, “Fabrication of Infrared Photodetectors Utilizing Lead Selenide Nanocrystals,” *Theses Diss.*, vol. 1805, Dec. 2016.

[53] A. O. Govorov, W. Zhang, T. Skeini, H. Richardson, J. Lee, and N. A. Kotov, “Gold nanoparticle ensembles as heaters and actuators: melting and collective plasmon resonances,” *Nanoscale Res. Lett.*, vol. 1, no. 1, p. 84, Jul. 2006.

[54] J. Chen, K. Žídek, M. Abdellah, M. J. Al-Marri, K. Zheng, and T. Pullerits, “Surface plasmon inhibited photo-luminescence activation in CdSe/ZnS core–shell quantum dots,” *J. Phys. Condens. Matter*, vol. 28, no. 25, p. 254001, Jun. 2016.

[55] D. B. Tice, M. T. Frederick, R. P. H. Chang, and E. A. Weiss, “Electron Migration Limits the Rate of Photobrightening in Thin Films of CdSe Quantum Dots in a Dry N2 (g) Atmosphere,” *J. Phys. Chem. C*, vol. 115, no. 9, pp. 3654–3662, Mar. 2011.

[56] C. Bohren and D. Huffman, “Absorption and Scattering by a Sphere,” in *Absorption and Scattering of Light by Small Particles*, Wiley-Blackwell, 2007, pp. 82–129.

[57] C. Mätzler, “MATLAB Functions for Mie Scattering and Absorption,” p. 19.

[58] P. B. Johnson and R. W. Christy, “Optical Constants of the Noble Metals,” *Phys. Rev. B*, vol. 6, no. 12, pp. 4370–4379, Dec. 1972.

[59] L. R. Hirsch *et al.*, “Nanoshell-mediated near-infrared thermal therapy of tumors under magnetic resonance guidance,” *Proc. Natl. Acad. Sci.*, vol. 100, no. 23, pp. 13549–13554, Nov. 2003.

[60] X. Huang and M. A. El-Sayed, “Gold nanoparticles: Optical properties and implementations in cancer diagnosis and photothermal therapy,” *J. Adv. Res.*, vol. 1, no. 1, pp. 13–28, Jan. 2010.

[61] K. R. B. Jr, A. G. Russell, P. A. Blake, and D. K. Roper, “Gold nanoparticles reduced in situ and dispersed in polymer thin films: optical and thermal properties,” *Nanotechnology*, vol. 23, no. 37, p. 375703, 2012.

[62] S. Ninomiya and S. Adachi, “Optical properties of cubic and hexagonal CdSe,” *J. Appl. Phys.*, vol. 78, no. 7, pp. 4681–4689, Oct. 1995.

[63] S. Ninomiya and S. Adachi, “Optical properties of wurtzite CdS,” *J. Appl. Phys.*, vol. 78, no. 2, pp. 1183–1190, Jul. 1995.

[64] M. Kerker, “Resonances in electromagnetic scattering by objects with negative absorption,” *Appl. Opt.*, vol. 18, no. 8, pp. 1180–1189, Apr. 1979.

[65] P. K. Jain, K. S. Lee, I. H. El-Sayed, and M. A. El-Sayed, “Calculated Absorption and Scattering Properties of Gold Nanoparticles of Different Size, Shape, and Composition: Applications in Biological Imaging and Biomedicine,” *J. Phys. Chem. B*, vol. 110, no. 14, pp. 7238–7248, Apr. 2006.

[66] L. Dyadyusha *et al.*, “Quenching of CdSe quantum dot emission, a new approach for biosensing,” *Chem. Commun.*, vol. 0, no. 25, pp. 3201–3203, Jun. 2005.

[67] E. Morales-Narváez, B. Pérez-López, L. B. Pires, and A. Merkoçi, “Simple Förster resonance energy transfer evidence for the ultrahigh quantum dot quenching efficiency by graphene oxide compared to other carbon structures,” *Carbon*, vol. 50, no. 8, pp. 2987–2993, Jul. 2012.

[68] T. Pons *et al.*, “On the Quenching of Semiconductor Quantum Dot Photoluminescence by Proximal Gold Nanoparticles,” *Nano Lett.*, vol. 7, no. 10, pp. 3157–3164, Oct. 2007.

[69] G. L. Liu, Y.-T. Long, Y. Choi, T. Kang, and L. P. Lee, “Quantized plasmon quenching dips nanospectroscopy via plasmon resonance energy transfer,” *Nat. Methods*, vol. 4, no. 12, pp. 1015–1017, Dec. 2007.

[70] S. Chang, X. Guo, and X. Ni, “Optical Metasurfaces: Progress and Applications,” *Annu. Rev. Mater. Res.*, vol. 48, no. 1, pp. 279–302, Jul. 2018.

[71] L. Huang *et al.*, “Helicity dependent directional surface plasmon polariton excitation using a metasurface with interfacial phase discontinuity,” *Light Sci. Appl.*, vol. 2, no. 3, p. e70, Mar. 2013.

[72] E. Karimi, S. A. Schulz, I. De Leon, H. Qassim, J. Upham, and R. W. Boyd, “Generating optical orbital angular momentum at visible wavelengths using a plasmonic metasurface,” *Light Sci. Appl.*, vol. 3, no. 5, p. e167, May 2014.

[73] Y. Yang, I. I. Kravchenko, D. P. Briggs, and J. Valentine, “All-dielectric metasurface analogue of electromagnetically induced transparency,” *Nat. Commun.*, vol. 5, p. 5753, Dec. 2014.

[74] T. Dong, X. Ma, and R. Mittra, “Modeling large nonuniform optical antenna arrays for metasurface application,” *J. Appl. Phys.*, vol. 114, no. 4, p. 043103, Jul. 2013.

[75] H. Li, G. Wang, H.-X. Xu, T. Cai, and J. Liang, “X-Band Phase-Gradient Metasurface for High-Gain Lens Antenna Application,” *IEEE Trans. Antennas Propag.*, vol. 63, no. 11, pp. 5144–5149, Nov. 2015.

[76] H. T. Miyazaki, T. Kasaya, M. Iwanaga, B. Choi, Y. Sugimoto, and K. Sakoda, “Dual-band infrared metasurface thermal emitter for CO2 sensing,” *Appl. Phys. Lett.*, vol. 105, no. 12, p. 121107, Sep. 2014.

[77] Q. Tang, M. Liang, and H. Xin, “Terahertz metasurface for potential live cell sensing application,” in *2013 IEEE Antennas and Propagation Society International Symposium (APSURSI)*, Orlando, FL, USA, 2013, pp. 2279–2280.

[78] Q. Wang *et al.*, “Broadband metasurface holograms: toward complete phase and amplitude engineering,” *Sci. Rep.*, vol. 6, p. 32867, Sep. 2016.

[79] D. Wen *et al.*, “Helicity multiplexed broadband metasurface holograms,” *Nat. Commun.*, vol. 6, p. 8241, Sep. 2015.

[80] J. Zhou *et al.*, “Application of metasurface description for multilayered metamaterials and an alternative theory for metamaterial perfect absorber,” Nov. 2011.

[81] K. Aydin, V. E. Ferry, R. M. Briggs, and H. A. Atwater, “Broadband polarization-independent resonant light absorption using ultrathin plasmonic super absorbers,” *Nat. Commun.*, vol. 2, p. 517, Nov. 2011.

[82] A. Boltasseva and H. A. Atwater, “Low-Loss Plasmonic Metamaterials,” *Science*, vol. 331, no. 6015, pp. 290–291, Jan. 2011.

[83] D. Doyle *et al.*, “Tunable Subnanometer Gap Plasmonic Metasurfaces,” *ACS Photonics*, vol. 5, no. 3, pp. 1012–1018, Mar. 2018.

APPENDIX A – LIST OF OPTICS USED

The order of the optics in the following list is the order encountered through the light path beginning with the laser.

Table 3 List of optics used

Part number	Name of optic	Company
CPS 532	532 nm laser	Thorlabs
FLO5532-10	Laser Line Filter	Thorlabs
LPVISE100-A	Linear Polarizer with A Coating	Thorlabs
MFF101	Motorized Flip Mount	Thorlabs
LA1908	Plano-convex lens f=500.0 mm	Thorlabs
ME1-G01	1" Diameter Round Aluminum Mirror	Thorlabs
NDL-25S-4	Step Variable ND Filter	Thorlabs
DMLP567	1" Longpass Dichroic Mirror, 567 nm cutoff	Thorlabs
46-405	50X Mitutoyo Plan Apo NIR Infinity Corrected Objective	Edmund Optics
FGL570	Colored Glass Longpass Filter	Thorlabs
FGL571	Colored Glass Longpass Filter	Thorlabs
FGL572	Colored Glass Longpass Filter	Thorlabs
TTL 200	Infinity Corrected 200 mm EFL Tube Lens	Thorlabs
ME1-G01	1" Diameter Round Aluminum Mirror	Thorlabs
MU035	CMOS Camera	Amscope
IsoPlane 160	Spectrometer	Princeton Instruments
PIX400	PIXIS 400-BRX CCD Camera	Princeton Instruments

APPENDIX B – MATLAB CODE

The following is the code used to take the .tiff files which are exported from Lightfield and turn them into data which can be copied into Microsoft Excel. As this is MATLAB code, the lines which have % in front of them are comment lines to explain the code. At the end of the code is a line which creates an array named ExcelDataExport. This array is copied into Excel for further analysis. There are also three figures created at the end of the code. These are used for visual verification of what the photobrightening looks like, as well as the central wavelength evolution over time. The other graph gives the central row used in the analysis.

```
% This program allows for the analysis of .tiff images.
% More specifically, this is designed to take images of
% quantum dot photobrightening and give enhancement values

clc;clf;clear all;

% This camera is 1340 pixels wide by 400 pixels tall
global XPixels
XPixels = 1340;
global YPixels
YPixels = 400;

% This is designed for a center wavelength of 650 nm.  If you are not using
% this, replace this file with a new wavelength reference file.
WavelengthReference = (importdata('Center Wavelength 650 nm.txt','\t'));

% Calls the tiff files in the directory.
% Note that this will only analyze files in the current directory.
tiffFiles = dir('*.tif');

% Identifies the number of files to be analyzed.
numFiles = length(tiffFiles);

% Creates a list of images that will be analyzed.
% Also creates a matrix for each image.
Images = cell(1,numFiles);
for k = 1:numFiles
    Images{k} = imread(tiffFiles(k).name);
end

% This part turns off a stupid warning that has no bearing on the program's
% efficacy.
warning('off', 'curvefit:fit:nonDoubleYData')
```

```
% This part creates a matrix of the quantum dot locations
% The program averages the columns together to determine the location
% of the greatest spot.  It then averages the few rows around that
% location to create a profile of the quantum dot emission. That emission
% is then fitted with a gaussian fit to determine the intensity and
% wavelength of the emission
Intensity = 1:numFiles;
Wavelength = 1:numFiles;
RowCenter = 1:numFiles;
Threshold = 64800;
% The following is an attempt at correction for camera saturation.
% If the camera is saturated on the last frame, the program uses the last
% unsaturated pixel in wavelength as the index, rather than a moving pixel.
% The problem is that it eliminates center wavelength reporting, but the
% data isn't useful in the event of saturation.
ColumnAverage = mean(Images{numFiles},2);
[Max,RowCenter] = max(ColumnAverage(:));
RowAverage = mean(Images{numFiles}([RowCenter-4:RowCenter+4],:));
saturation = 0;
if max(RowAverage) > Threshold
    saturation = 1;
    IndexPixel = find(RowAverage >= Threshold,1, 'first')-5;

    for i = 1:numFiles
        ColumnAverage = mean(Images{i},2);
        [Max,RowCenter] = max(ColumnAverage(:));
        RowAverage = mean(Images{i}([RowCenter-4:RowCenter+4],:));
        RowList(i) = RowCenter;
        Intensity(i) = mean(RowAverage(IndexPixel-
1):RowAverage(IndexPixel+1));
    end
else
    for i = 1:numFiles
        ColumnAverage = mean(Images{i},2);
        [Max,RowCenter] = max(ColumnAverage(:));
        RowAverage = mean(Images{i}([RowCenter-4:RowCenter+4],:));
        RowList(i) = RowCenter;
        f = fit(WavelengthReference,transpose(RowAverage),'gauss1');
        coeff = coeffvalues(f);
        Intensity(i) = coeff(1);
        Wavelength(i) = coeff(2);
    end
end
% Photobrightening is defined here to be the percent increase above the
% original value
Photobrightening = (Intensity/Intensity(1)-1)*100;
plot(Intensity)
figure
plot(RowList)
ExcelDataExport = transpose(Intensity);
figure
plot(Wavelength)
WavelengthExport = transpose(Wavelength);
```

APPENDIX C – SURFACE PLASMON DAMPING EFFECTS DUE TO TI ADHESION LAYER IN INDIVIDUAL GOLD NANODISKS[19]

While, in the course of this work, plasmonics have been discussed as to their effects, what has been lacking in the discussion has been any real mention of designed plasmonic nanostructures, such as those fabricated by electron-beam lithography. The process of e-beam lithography is used to create nanoscale devices below the limit of optical lithography. The pattern is etched into a layer of, in this case, PMMA, and then the metal is deposited via electron beam vapor deposition. For many cases, the substrate being used is silicon and the plasmonic material is gold. Due to the low adhesive bond between gold and silicon, another material such as titanium must be used as an adhesive layer. This layer will alter the plasmonic properties of the device that is used, so understanding how the thickness of the adhesive layer will affect the outcome is vital.

This paper works to answer this question using COMSOL simulations. The target geometries were nanodisks of various diameters, all of the same 15 nm thickness of gold surrounded by a medium with a refractive index equivalent to the average index of refraction between silicon and air. The thickness of the titanium adhesion layer was varied from 0 to 5 nm and the scattering, absorption, and extinction coefficients were simulated, along with the spectral broadening and shifting. For the scattering, absorption, and extinction coefficients, it was found that each of them is decreased with the addition of a titanium layer, and the decrease was made greater the thicker the layer of titanium. The sharpest drop occurs for the scattering coefficient with the addition of a titanium layer, dropping by about a factor of 2, while the absorption coefficient drops from about 3.5 to 3. In neither case does the addition of a titanium layer cause improved performance. This decrease in the amplitude is due to the damping of the plasmons by the titanium. Results from the paper are below in Figure 42.

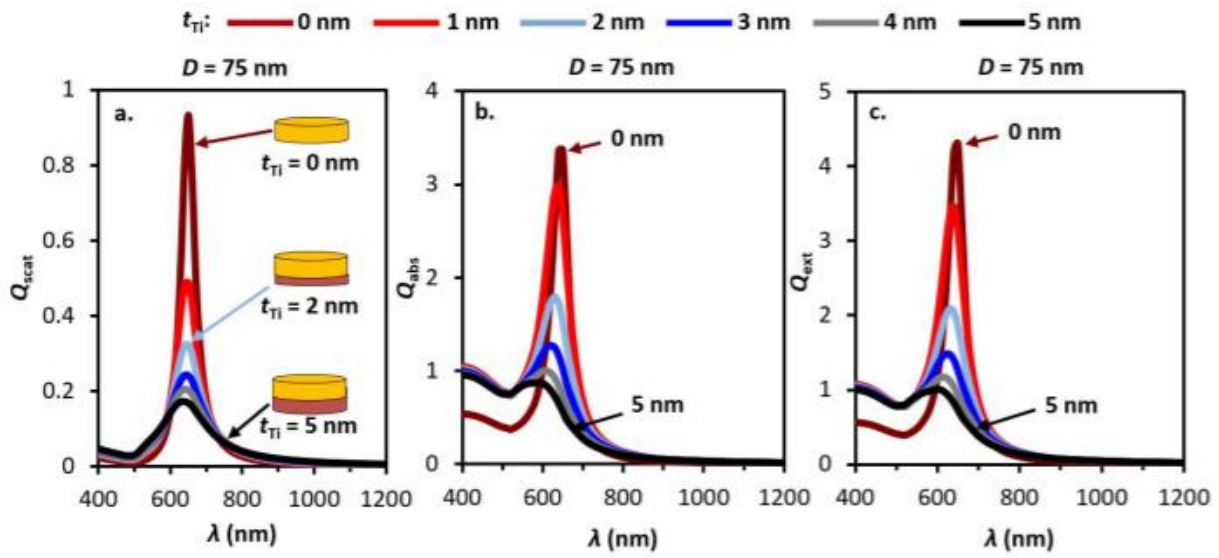

Figure 42 Simulated (a) scattering, (b) absorption, and (c) extinction spectra for 75 nm diameter gold nanodisks of 15 nm thickness with certain thicknesses of titanium. The addition of titanium results in the decrease of the spectral amplitudes, as well as the blueshifting of the absorption and extinction spectra. Figure from [19].

In addition to the scattering coefficient, the peak wavelength also blueshifts for both the scattering and absorption spectra. This blueshift is most prominent in the extinction coefficient, expected as extinction is a combination of the absorption and scattering spectra. There is also a significantly greater blueshift in the absorption spectrum than the scattering spectrum, making it significantly easier to separate the scattering and absorption peaks by adding titanium. The blueshifting of the spectral peaks is accompanied by a broadening of the spectral lines, as determined by an increase in the full-width at half maximum (FWHM) of the spectra. These findings will, in future fabrication, be instrumental in tuning the response of plasmonic structures for desired tasks.

APPENDIX D – CALCULATED THICKNESS DEPENDENT PLASMONIC PROPERTIES OF GOLD NANOBARS IN THE VISIBLE TO NEAR-INFRARED LIGHT REGIME[5]

The thickness of the titanium having been thoroughly investigated, the questions now turn to how the thickness of the gold itself affects the plasmonic properties of the devices being manufactured. While it may be tempting to think of the nanodevices as being largely 2-dimensional, an idea which is fairly accurate in the case of large-scale arrays, the thickness of the plasmonic material used is still an important parameter, both because it contributes to the plasmonic response of the design and because of manufacturing considerations. Gold is expensive, so the less that is used, the cheaper the device. In the case of this paper, the test case was gold nanobars (rectangular prisms) in the near-infrared range.

Like the previous paper discussed, the analysis of the plasmonic properties is performed using COMSOL. Also like the previous paper, an effective index of refraction was used to simplify the calculations involved. In a departure from the findings of the last paper however, the titanium adhesion layer was not simulated, again to simplify the calculations. The simulations were designed to analyze the effects of two parameters, the thickness of the nanobars and the bevels of the corners. The reason for the simulation of the bevel is to more accurately simulate the real features of a nanobar fabricated with electron beam lithography, as the sharp corners of rectangular prisms are not possible to fabricate; there will always be a curve of some non-zero radius on the edges of the nanobars.

The first parameter studied is the thickness of the gold. With an increase of the thickness of the gold there is a blueshift in the absorption spectrum as well as a decrease in the amplitude of

the peak absorption. This result is identical for both transverse and longitudinal polarizations of incoming light, as shown in

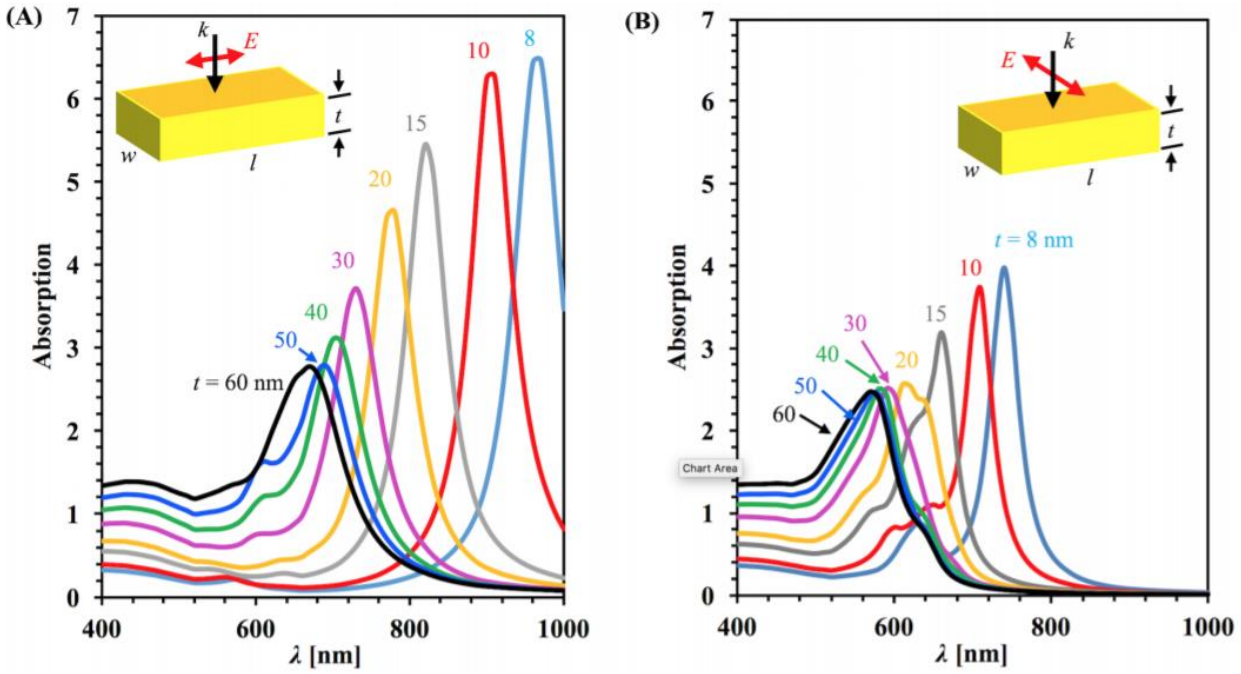

Figure 43 Simulated absorption spectra for various thicknesses (t) of nanobars. The absorption spectra were simulated for both the (A) longitudinal and (B) transverse polarization directions. The increasing thickness leads to a decrease in both the amplitude and peak wavelength value for both directions. Image taken from [5].

The blueshifting of the absorption peak is due to the increased separation of the charges in the vertical direction, leading to higher order modes as the dipole begins to exhibit properties of quadrupole and higher multipole moments. Similar behavior is exhibited by the optical enhancement factor, as shown in [5].

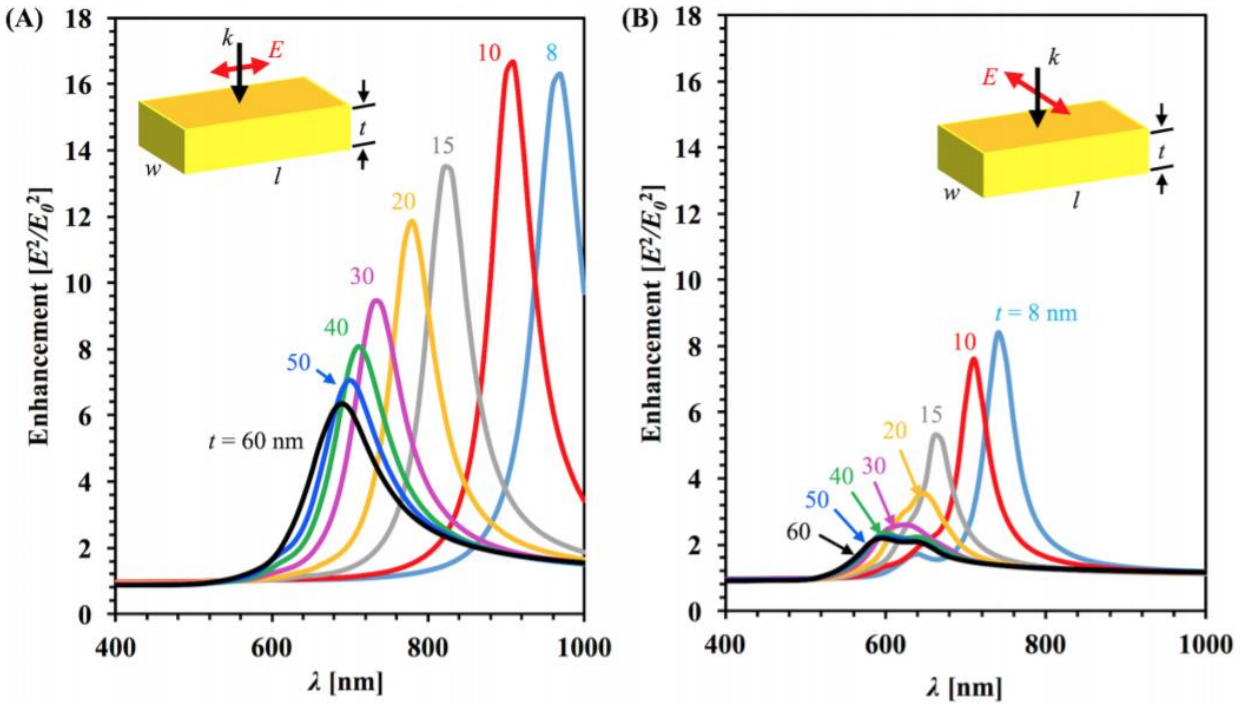

Figure 44 The optical enhancement factor as simulated for gold nanobars of various thicknesses for both the (A) longitudinal and (B) transverse polarization directions. The increasing thickness leads to both a decrease in the maximum value of the enhancement factor and a blueshift in the peak enhancement wavelength. Image taken from [5].

Having now determined that both the absorption amplitude and the enhancement factor will be decreased with the increase of thickness of the nanobar, attention can now be given to how the addition of a bevel will change the behavior. The bevel is an unavoidable part of the fabrication of nanobars using electron beam lithography but it is not commonly simulated in studies. With the addition of the beveled edges the nanobars have the enhancement factors and the peak enhancement wavelength lessened. This decrease occurs for both the longitudinal and transverse polarization directions, and by about the same amount for each. This is shown in Figure 45.

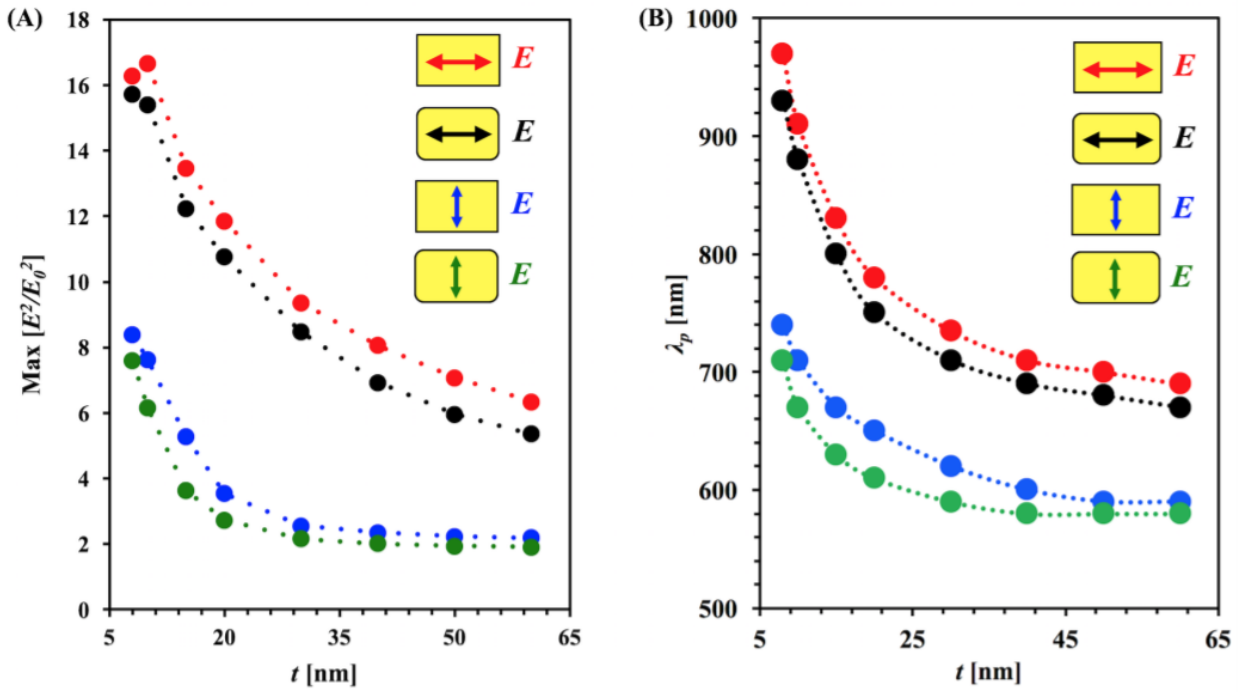

Figure 45 The simulated (A) enhancement factor and (B) peak enhancement wavelength for both beveled and non-beveled nanobars for both polarization directions for various thicknesses of nanobars. Image from [5].

The graphs indicate that there is a significant difference between the enhancement factors and peak wavelengths for the beveled and non-beveled cases. However, despite that fact, the predictable relationship between the two cases means that it may not be critical to simulate the beveled edges if the goal is to analyze the general behavior. That being said, the inclusion of the beveled edges will still be necessary if the goal is to design nanostructures for specific wavelengths.

APPENDIX E – TUNING INFRARED PLASMON RESONANCE OF BLACK PHOSPHORENE NANORIBBON WITH A DIELECTRIC INTERFACE[20]

While most papers investigating aspects of plasmonic behavior restrict their inquiries to noble metals such as gold and silver, those metals are not the only materials capable of supporting plasmon resonances. One of the materials which has been gaining recognition is phosphorene, a two-dimensional ribbon structure of phosphorus. This is capable of sustaining plasmons like metals, but in much longer wavelengths. This paper uses theoretical and computational models to explore some of the plasmonic properties of black phosphorus, such as the polarization dependence, a feature not present in metals due to their radially symmetric nature. Unlike metals, or graphene, another 2-dimensional material with potential plasmonic applications, black phosphorus has two distinct geometries depending on the orientation – the armchair and zigzag directions. The different geometries give different behaviors when exposed to light polarized in that direction.

The nature of 2-dimensional materials means that the ribbons of black phosphorus need to be supported by a substrate. The index of refraction of this substrate alters the plasmonic modes supported by the black phosphorus. To study this effect, a simulated black phosphorus ribbon was laid on top of a substrate with a period of 250 nm. Beneath the substrate is placed a gold reflector to confine the enhanced light within the simulation space, while above the black phosphorus ribbons is placed air. The width of the nanoribbon is of great concern, as is the direction of the polarization of the light. These were studied via computational simulations and the results are below in Figure 46.

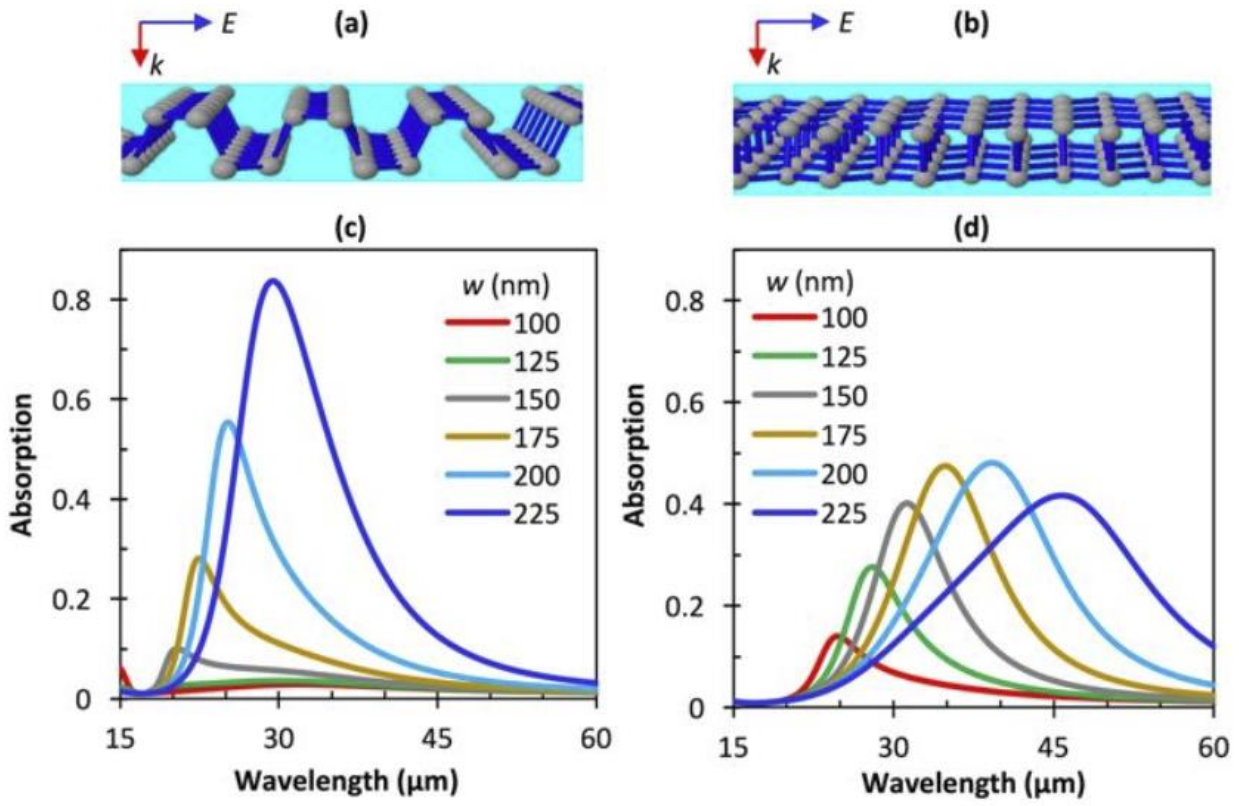

Figure 46 The (a) armchair and (b) zigzag directions of black phosphorus illustrated. The absorption spectra for the (c) armchair and (b) zigzag directions of black phosphorus for select widths of nanoribbon. Image used with permission from [20].

There is a stark difference displayed between the two directions of polarization. With the light polarized in the armchair direction the peak absorption value increases with the width of the ribbon in every case, a relation not shared by the orthogonal polarization. Additionally, the values of absorption are, in nearly every case, lower in the armchair case than in the zigzag direction, with the exception of the 200 nm and 225 nm widths. Nevertheless, both polarization directions do show a redshift as the width increases, a pattern shared by their metallic counterparts. The findings presented above are important but provide a misleading idea of what devices featuring black phosphorus will look like. One of the characteristics of black phosphorus is its reaction to oxygen, which causes degradation of the structure. Another is the reaction to water which can also

cause the alteration of the structure and eventual destruction. The solution is to surround the black phosphorus with some form of dielectric shielding, thereby preventing the environmental factors from damaging the ribbons while still allowing the light to pass through to the ribbons. One of the materials under consideration is hexagonal boron nitride, so chosen due to the fact that it does not react with most materials and is durable. Additionally, the thickness of the layer of hexagonal boron nitride can be carefully controlled. To test the effects, same simulations as before were performed except that a layer of hexagonal boron nitride was placed over the substrate and black phosphorus ribbons. The absorption spectra resulting from the arranged geometries are shown below in Figure 47.

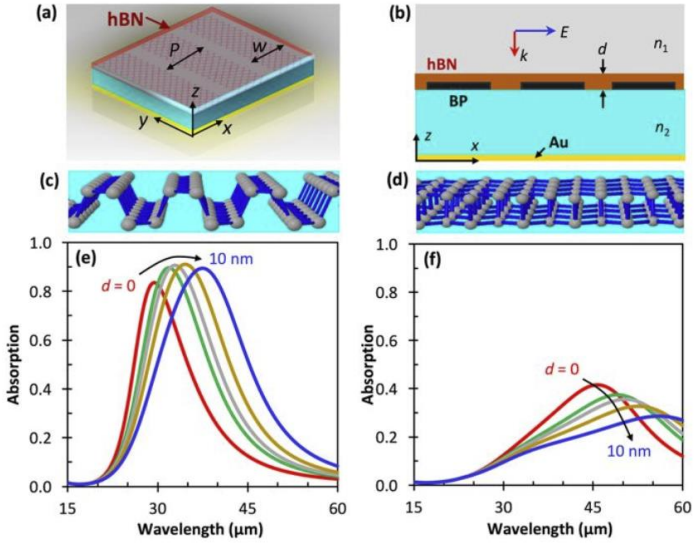

Figure 47 (a) A 3-dimensional view of the simulation under consideration. (b) A 2-dimensional view of (a). (c) and (d) show views of the armchair and zigzag directions respectively. (e) and (f) show the absorption in the armchair and zigzag directions respectively. Both directions exhibit redshifting as the depth *d* increases. Image taken from [20].

By increasing the number of layers of hexagonal boron nitride, the plasmonic peaks for both the armchair and zigzag directions shift toward longer wavelengths. There is, however, a noticeable difference between the absorption value trends for the two directions. In the case of

the zigzag direction, the absorption strictly decreases as the depth of the hexagonal boron nitride increases. This is not the case for the armchair direction. In that case, the absorption values tend to increase until a critical value is met. Taken together, the findings of the paper present a basis for future research applications requiring plasmonic peaks in the mid to far infrared wavelength range.

APPENDIX F – CURRENT DENSITY CONTRIBUTION TO PLASMONIC ENHANCEMENT EFFECTS IN METAL-SEMICONDUCTOR-METAL PHOTODETECTORS[15]

Basic research like that discussed in the previous papers is vital for progress in any field, but there comes a time when the basic research must give way to applications. One of the main applications of plasmonics, as has been pointed out in countless papers, is that of photodetectors. Briefly, metal-semiconductor-metal photodetectors use photoinduced current to determine when light is hitting the detector and the sensitivity of the photodetector is dependent on the amount of photocurrent which can be moved by a given voltage. The more photocurrent moveable via a lower voltage, the higher the signal-to-noise ratio of the detector, and the lower the threshold needed to determine that photons are present. The more photons which hit regions of the detector that have the necessary voltage, the greater the induced photocurrent. Maximizing the photons in the given regions of useful current is therefore vital to sensitivity, and this is where plasmonics shines.

The feature of plasmonics which is of interest is the ability to effectively move electromagnetic fields from locations undesired to locations more useful. By adding additional material to a photodetector such as that described above it is possible to harness more of the light for inducing photocurrent. The additional material is, in this case, formed into certain geometries which can be tuned to respond best to certain wavelengths of light, causing the enhancement of the field in the regions necessary for photodetection. An example of this setup is shown in Figure 48.

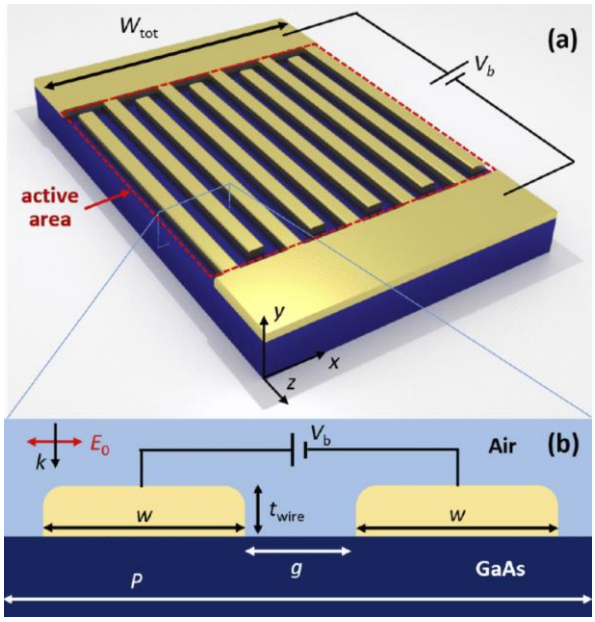

Figure 48 (a) An illustration of a plasmonically enhanced metal-semiconductor-metal photodetector. The structure is made of gold and placed on gallium arsenide. (b) a 2-dimensional view of two of the arms of the photodetector which will be used as the basis for the computational simulations. Image used with permission from [15].

Figure 48 (b) shows the simulation geometry used for calculating the effects of this design. The thickness of the wires and the gap between the electrodes were kept at constant values along with the wavelength of the incoming light. The period of the device was set to twice the width plus twice the gap size and mirrored boundary conditions were imposed to simulate the device. There were two separate simulations run on this system. The first is the same simulation run before, showing the electric field enhancement values in order to figure out the locations of greatest enhancement and how that enhancement changes based on the wire width. The second is a current density simulation. This uses a voltage between the electrodes to determine the current flow. The results of the simulations are shown in Figure 49.

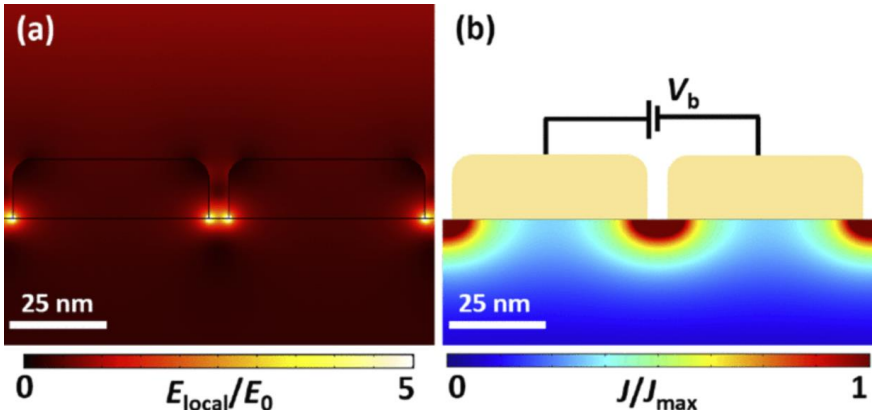

Figure 49 (a) The electric field enhancement due to the electrodes of the photodetector. (b) The current density through the substrate due to the bias voltage between the electrodes. Image used with permission from [15].

Clear from the above image is the fact that the maximum electric field enhancement is in a similar location to the maximum current density. Unfortunately, due to the inner workings of the software, it is not possible to combine the two simulations, so another method must be devised to determine the effect of the incoming light on the current. Therefore, a weighted optical enhancement was determined by weighting the optical enhancement value by the current density at the same location. This weighted optical enhancement value represents the useful enhancement for each pair of electrodes, and from there a value for the total enhancement of the device, *G*, can be determined. Having done this, the enhancement of the device can be optimized by changing certain parameters such as the wire width or gap width as shown in Figure 50.

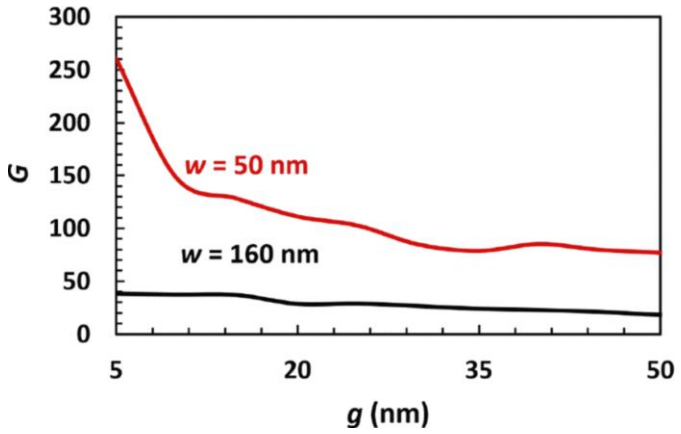

Figure 50 The device enhancement of two different wire widths, 50 nm (red) and 160 nm (black), for a range of gap widths. Image used with permission from [15].

From the graph shown, it is clear that the smaller gap and wire widths lead to a significantly greater enhancement of the device, meaning that more current will flow with a lower level of light, leading to increased sensitivity in photodetectors.

APPENDIX G – PERMISSIONS TO REPRODUCE FIGURES

Copyright Clearance Center RightsLink®

Home | Create Account | Help

ACS Publications
Most Trusted. Most Cited. Most Read.

Title: Tunable Subnanometer Gap Plasmonic Metasurfaces
Author: Dennis Doyle, Nicholas Charipar, Christos Argyropoulos, et al
Publication: ACS Photonics
Publisher: American Chemical Society
Date: Mar 1, 2018
Copyright © 2018, American Chemical Society

LOGIN

If you're a copyright.com user, you can login to RightsLink using your copyright.com credentials.

Already **a RightsLink user** or want to learn more?

PERMISSION/LICENSE IS GRANTED FOR YOUR ORDER AT NO CHARGE

This type of permission/license, instead of the standard Terms & Conditions, is sent to you because no fee is being charged for your order. Please note the following:

- Permission is granted for your request in both print and electronic formats, and translations.
- If figures and/or tables were requested, they may be adapted or used in part.
- Please print this page for your records and send a copy of it to your publisher/graduate school.
- Appropriate credit for the requested material should be given as follows: "Reprinted (adapted) with permission from (COMPLETE REFERENCE CITATION). Copyright (YEAR) American Chemical Society." Insert appropriate information in place of the capitalized words.
- One-time permission is granted only for the use specified in your request. No additional uses are granted (such as derivative works or other editions). For any other uses, please submit a new request.

If credit is given to another source for the material you requested, permission must be obtained from that source.